Title	STUDIES OM THE ANODIC CHARACTERISTICS OF MANGANESE OXIDES
Author(s)	森田, 昌行
Citation	大阪大学, 1980, 博士論文
Version Type	VoR
URL	https://hdl.handle.net/11094/1743
rights	
Note	

STUDIES ON THE ANODIC CHARACTERISTICS

OF MANGANESE OXIDES

1980

MASAYUKI MORITA

Department of Applied Chemistry

Faculty of Engineering

Osaka University

STUDIES ON THE ANODIC CHARACTERISTICS

OF MANGANESE OXIDES

1980

MASAYUKI MORITA

Department of Applied Chemistry

Faculty of Engineering

Osaka University

PREFACE

The work of this thesis was done under the guidance of Professor Dr. Hideo Tamura at Osaka University for five years since 1975.

Masayuki Morita

Suita, Osaka

January, 1980

CONTENTS

.

GENERAL INTRODUCTION

The functions required of electrodes are fairly easy to
define.   In general, the electrodes for industrial electrolysis
should be: (1) a good conductor, (2) an efficient electrocata-
lyst for the reaction in question, (3) corrosion resistant and
otherwise free from chemical attack, and (4) mechanically rigid
[1].   Besides these, availability and reasonable cost are also
required for the electrode materials in most cases.   The sub-
stances subjecting to the anodic dissolution are particularly
ruled out from possible anode materials with a few exceptions.
In most cases, however, it is very difficult to ensure the
sufficient chemical stability of the anodes under highly polar-
ized conditions because of the electrochemical oxidative affinity.
An anode material satisfying most of the above requirements
is the insoluble anode, so-called DSA, which has recently been
introduced into the chlor-alkali industry [2].   It consists of
the film of the noble metal oxides supported on the valve metal
substrate such as titanium, and is excellent in the catalytic
activity and in the stability for the brine electrolysis compared
with the graphite anode [3].   In addition to the practical
works, many fundamental ones have been performed in the chloride
solutions on the electrochemical behaviours of noble metals [4,5]
and their alloy [6-10] and oxides [11-22] which are main com-
ponents in the DSA.
On the other hand, the development of anode materials is of
special importance in water electrolysis and other electrolytic

- 1 -

processes, not to mention brine electrolysis, because the oxygen overvoltage is the chief cause of energy losses in such devices [23]. Thus, the DSA is expected to be applied widely to the other electrolytic fields in future, and, in fact, the oxygen evolution reaction on the DSA has been studied increasingly [24-29]. However, most of the electrocatalysts so far employed in the DSA consist of the noble metal oxides, especially ruthenium dioxide, and hence it has been desired to use the oxides of base metals from the standpoints of economy and resources.

Manganese dioxide, which is abundantly present and inexpensive, has been predominantly used in a dry cell as an active material. Therefore, its solid state properties [30] and the cathodic discharge characteristics [31] have been studied fairly in detail. However, there has been no systematic work with a view to using manganese dioxide and related oxides as anodes for electrolytic processes, in spite of the publication of the recent brief papers [32-35] and the data of activation energies for the anodic evolution of oxygen and chlorine [36].

From the above viewpoints, it was intended in this work to evaluate the use of manganese oxides as a new anode material for electrolytic processes. Thus, the manganese oxide anodes primarily containing manganese dioxide were prepared by the thermal decomposition method, and their anodic characteristics were investigated in aqueous solutions. In particular, the anodic evolution reactions of oxygen and chlorine on the manganese oxides were discussed in detail. The contents of this thesis is composed of the following four chapters.

In chapter 1, the anodic characteristics of the film-type

electrodes of manganese oxides are clarified, especially with regard to the anodic evolution of oxygen. Chapter 2 describes the study on the anodic behaviours of massive manganese oxides in order to elucidate the intrinsic properties of the manganese oxides anodes in aqueous solutions. In chapter 3, the influence of the noble metals doped in the massive manganese dioxide anode is examined on the anodic evolution of chlorine. And the electrocatalytic activities of the mixed Mn-Pd oxides for the chlorine electrode reaction are discussed in chapter 4.

Most results of the investigation presented in this thesis have already been published in the following six papers.

1. The Anodic Characteristics of Manganese Dioxide Electrodes Prepared by Thermal Decomposition of Manganese Nitrate

    M. Morita, C. Iwakura and H. Tamura,

    Electrochim. Acta, 22, 325 (1977).

2. The Anodic Characteristics of Modified Mn Oxide Electrode: Ti/RuOx/MnOx

    M. Morita, C. Iwakura and H. Tamura,

    Electrochim. Acta, 23, 331 (1978).

3. The Anodic Characteristics of Massive Manganese Oxide Electrodes

    M. Morita, C. Iwakura and H. Tamura,

    Electrochim. Acta, 24, 357 (1979).

4. The Anodic Characteristics of the Massive β-MnO$_2$ Doped with Noble Metals in Sodium Chloride Solution

    M. Morita, C. Iwakura and H. Tamura,

    Electrochim. Acta, 24, 639 (1979).

5. The Anodic Characteristics of Mixed Mn-Pd Oxide Electrodes

   M. Morita, C. Iwakura and H. Tamura,

   Denki Kagaku, in press.

6. The Electrocatalytic Activities of the Pd-Doped MnO_2 for the
   Chlorine Evolution Reaction

   M. Morita, C. Iwakura and H. Tamura,

   Electrochim. Acta, in contribution.

CHAPTER 1

THE ANODIC CHARACTERISTICS OF FILM-TYPE MANGANESE OXIDE ELECTRODES

1. INTRODUCTION

Since Konovalov et al [37] first attempted to use a manganese dioxide film as an anode for electrolytic processes, ·there have been some brief papers [32-35] concerning manganese dioxide film anodes supported with metal substrates such as titanium. However, no consistent information has been available for anodic characteristics of the manganese dioxide film, because its anodic properties were markedly changed by the preparative condition of the film and the substrate of the electrode.

Accordingly, in this chapter, manganese oxide (MnOx) films were prepared by thermal decomposition of manganese (II) nitrate on the metal substrates such as titanium, platinum and RuOx-coated titanium, and their anodic characteristics were investigated in aqueous solutions. Especially, the kinetics and the electrocatalytic activity for the anodic evolution of oxygen were discussed in detail.

2. EXPERIMENTAL

Film-type electrodes of manganese oxide were prepared by a thermal decomposition method [38,39]. A titanium plate (12.5 x 20 x 0.5mm) or a platinum plate (12.5 x 20 x 0.2mm) was used as a substrate. 0.1M $Mn(NO_3)_2$ in an aqueous solution was applied to one side of the substrate in several sequential coatings. After each coating, the solution was dried at a moderate temperature (below 100°C in a drying oven) and then decomposed in a furnace at 170°C for 10min. The total amount decomposed was 10^{-5}mol Mn/cm^2. The sample was cooled between each of the coatings. After the final coating, it was heated to 450°C for 1h and then cooled.

In some cases, the preliminary coatings of ruthenium oxide on a titanium substrate, or the introduction of a ruthenium oxide film as an intermediate layer into the Ti/Mn oxide inter-face, was accomplished by thermal decomposition of ruthenium trichloride [24]. A proper quantity of 10^{-2}M or 10^{-3}M $RuCl_3$-20% HCl aqueous solution was used for this procedure. The ruthenium oxide loadings ranged from 5×10^{-8} to 1×10^{-6}mol Ru/cm^2.

The composition of the manganese oxide was determined by X-ray diffraction method and found to be the mixture of so-called β-MnO_2 and α-Mn_2O_3. On the other hand, the principal constitu-ent of the intermediate ruthenium oxide layer was identified as RuO_2. Hereinafter, the test electrodes will be referred to as Ti/MnOx, Pt/MnOx and Ti/RuOx/MnOx electrodes for convenience.

An all-Pyrex glass H-type cell with Teflon stoppers was

used as an electrolytic cell. The counter electrode was a platinum sheet (20 x 25mm) and the reference electrode was a hydrogen electrode (he) in the same solution, a mercurous sulfate electrode (Hg/Hg_2SO_4, 0.5M H_2SO_4), a mercuric oxide electrode (Hg/HgO, 1M KOH) or a saturated calomel electrode (sce), appropriate to the electrolytes.

Each electrolyte was prepared from special grade reagent and twice-distilled water, and was purified by electrolysis over 50h before use. All gases were purified by passing through the same train as the one described in the literature [38].

The polarization characteristics of the test electrodes were measured under the potentiostatic condition with an usual potentiostat and an electronic polyrecorder, or under the galvanostatic condition with a dc constant current power supply and a digital voltmeter. In the latter case, iR drops were corrected by using an interrupter. The current densities shown in this work will be indicated by the apparent one based on the geometric area ($1cm^2$) although the electrochemically working area of each electrode was estimated by the surface chelation method [40]. All measurements except for the experiments of the temperature dependence were carried out at 30°C.

3. RESULTS AND DISCUSSION

1. Polarization characteristics

The current-potential curves obtained potentiostatically on some Ti/MnOx electrodes in 0.5M H_2SO_4 are shown in Fig. 1.
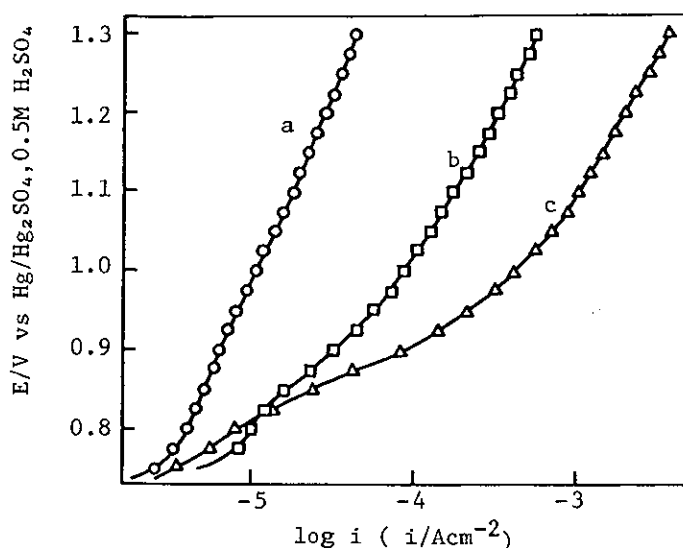
Fig. 1. Current-potential curves of Ti/MnOx in 0.5M H_2SO_4.
a: 450°C, b: 350°C, c: 250°C.

It can be seen from this figure that the anodic current decreases with increasing temperature of the final heat treatment in the electrode preparation. This temperature dependence of the current is attributable to the existence of a TiO_2 layer between the Ti substrate and the Mn oxide which is formed during the heat treatment, since it is considered that the thickness of the TiO_2 layer and then the electric resistance or the ohmic drop in the bulk of the electrode increases with increasing the temperature of the heat treatment. This interpretation was qualitatively supported by the electric resistances of these electrodes measured in mercury pool; eg Ti/MnOx (350°C): $0.62\Omega cm^2$, Pt/MnOx (450°C): $0.0064\Omega cm^2$. The existence of the TiO_2 layer, however, contributes to the adhesion of the catalytic oxide to the Ti substrate. It has been reported that $\beta-MnO_2$ which is the principal constituent of MnOx in the electrode possesses rutile structure [41] and that TiO_2 produced by thermal decomposition

has also rutile mixed with anatase [42,43]. The Ti/MnOx electrode, consequently, is superior in adhesion to Pt/MnOx, results for which are described later.

The anodic polarization characteristics of Pt/MnOx electrode are compared with that of the bright Pt electrode in Fig. 2. The Pt substrate was selected for the reason that the thick oxide film is hardly formed by the heat treatment and the electronic conductivity of the oxide is relatively high. Evidently the Pt/MnOx electrode has a considerably lower overvoltage for the oxygen evolution than the bright Pt electrode and the current at the given potential is much higher by about order two on the former than on the latter. Furthermore, anodic dissolution of the Mn oxide was not observed on a Pt/MnOx electrode. It has also become apparent that the polarization curve is scarcely affected by the change in the catalyst loading on the substrate.

Another practical approach to solve the problem of the high electric resistivity of the TiO_2 layer at the Ti/MnOx
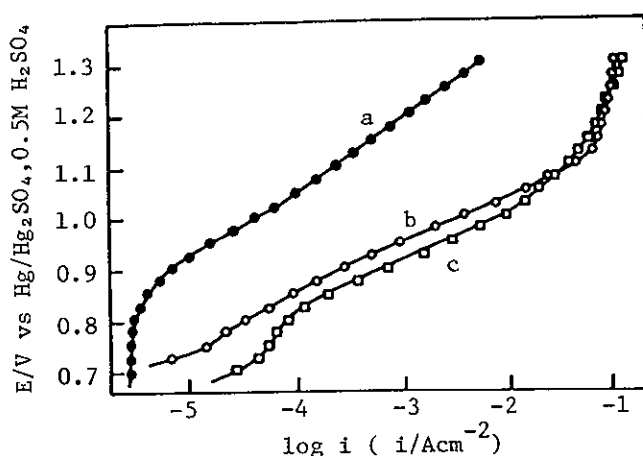

Fig. 2. Current-potential curves of Pt/MnOx in 0.5M H_2SO_4.
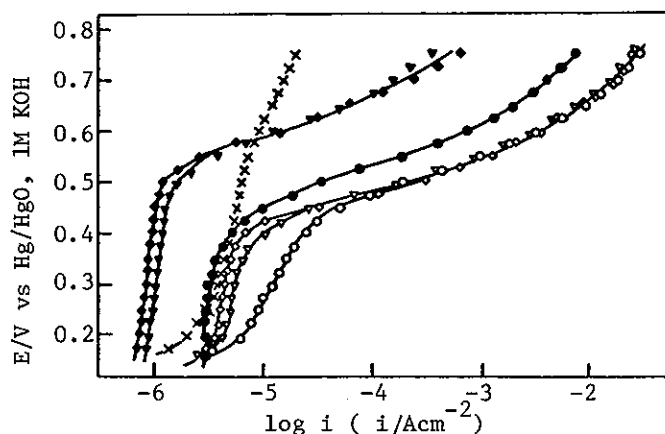a: bright Pt, b: 10^{-5} mol Mn/cm^2, c: 10^{-4} mol Mn/cm^2.

Fig. 3. Current-potential curves in 1M KOH.
○: $Ti/RuOx(1 \times 10^{-6})/MnOx(1 \times 10^{-5})$,
◇: $Ti/RuOx(1 \times 10^{-7})/MnOx(1 \times 10^{-5})$,
▽: $Ti/RuOx(5 \times 10^{-8})/MnOx(1 \times 10^{-5})$,
●: $Ti/RuOx(1 \times 10^{-6})$, ◆: $Ti/RuOx(1 \times 10^{-7})$,
▼: $Ti/RuOx(5 \times 10^{-8})$, ✕: $Ti/MnOx(1 \times 10^{-5})$.
The values in a parenthesis indicate the oxide
loadings in mol/cm^2.

boundary is that the Ti substrate is covered with suitable
conductive materials such as Ru oxide prior to the Mn oxide
coating. Figure 3 shows the current-potential curves obtained
on some Ti/RuOx/MnOx electrodes with the different amounts of
Ru oxide, compared with the Ti/MnOx and Mn oxide-free Ti/RuOx
electrodes. The shape of the curve and the magnitude of
current density are little affected by the change in the amount
of Ru oxide from 5×10^{-8} to 1×10^{-6} mol Ru/cm^2.

It is evident from this figure that the Ru oxide serves
effectively as expected, since the current densities on the
Ti/RuOx/MnOx electrodes are higher by a few orders of magnitude
than that on the Ti/MnOx electrode. On the other hand, the
current densities on the Ti/RuOx electrodes where the Ru oxide

itself acts as a catalyst for the oxygen evolution reaction are
considerably lower than those on the Ti/RuOx/MnOx electrodes
because of the small amounts of the RuOx catalyst.   According
to these results, it has become apparent that the presence of
the Ru oxide decreases the electric resistivity or the potential
barrier in the bulk of the electrode and that the anodic oxygen
evolution occurs on the surface of the Mn oxide.   In addition,
it is emphasized that no anodic dissolution of the MnOx catalyst
was observed in this work.   For the later experiments, the
amount of Ru oxide in the Ti/RuOx/MnOx electrode was kept
constant at 1×10^{-7} mol Ru/cm^2.

In order to clarify how the Ru oxide contributes to the
improvement of the electric characteristics in the bulk of the
electrode, the in-depth analyses of the electrode constituents
were carried out by means of a secondary ion mass spectrometry
(SIMS).   The X-ray diffraction analyses were also conducted
for the oxides produced by the solid state reactions of TiO_2-
MnO_2 and TiO_2-RuO_2 systems.   These experimental results lead
to the presumption of the composition for the metal-oxide
boundary regions of Ti/MnOx and Ti/RuOx electrodes, as shown in
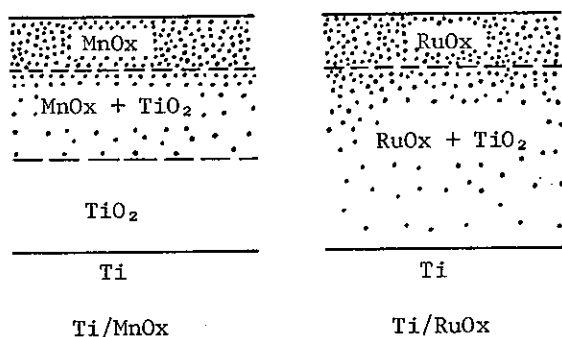Fig. 4.   In contrast to the fact that the thermal decomposition

Fig. 4.   Presumable models for the composition of
the film-type electrodes.

of RuCl$_3$ on a titanium substrate easily leads to the formation

of mixed crystals, or solid solutions, of RuOx and TiO$_2$ [3,16,

42,44], it seems likely that the solid solutions of MnOx and

TiO$_2$ are difficult to be formed during the preparation of the

Ti/MnOx electrode. It has been reported that β-MnO$_2$ is hardly

soluble in TiO$_2$ [45].

Both RuO$_2$ and β-MnO$_2$, which are the principal constituents

of Ru oxide and Mn oxide in the electrode, respectively, possess

the rutile structure crystalographically. The principal con-

stituent of the TiO$_2$ film formed during thermal decomposition

is also rutile-type [42,43]. However, the difference in solu-

bility for TiO$_2$ between β-MnO$_2$ and RuO$_2$ may related to the

difference in dimension of the crystal lattice (TiO$_2$: a = 4.594,

c = 2.958Å [46,47], β-MnO$_2$: a = 4.398, c = 2.867Å [47], RuO$_2$:

a = 4.519, c = 3.116Å [46]). The volume of the unit cell of

each oxide is calculated to be 62.4 for TiO$_2$, 55.5 for β-MnO$_2$

and 63.6Å^3 for RuO$_2$. Thus, the lattice dimension of TiO$_2$

approximately equals to that of RuO$_2$ but greatly differs from

that of β-MnO$_2$. Therefore, this difficulty in the formation

of solid solutions of MnOx and TiO$_2$ may result in the existence

of a pure TiO$_2$ layer in the bulk of Ti/MnOx electrode, and

hence the characteristics of the electrode are extremely affected

by the pure TiO$_2$ layer which has a high resistivity and potential

barrier.

Figure 5 shows the variation of potential with time during

the anodic polarization at 10mA/cm^2 on a Pt/MnOx electrode in

0.5M H$_2$SO$_4$ and 1M KOH. The potential was virtually invariant,

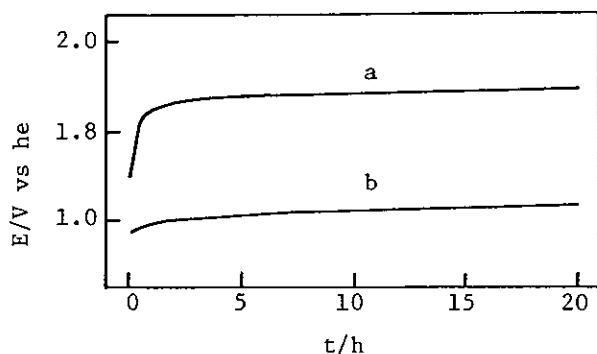or only less than 30mV for 20h, in 1M KOH, whereas in 0.5M H$_2$SO$_4$

Fig. 5. Potential-time curves of Pt/MnOx
under anodic polarization at 10mA/cm^2.
a:in 0.5M H$_2$SO$_4$, b:in 1M KOH.

it changed to the anodic side by about 150mV during first hour
after the polarization was started.   Furthermore, such polar-
ization in 0.5M H$_2$SO$_4$ resulted in weakening the mechanical
bonding of the catalytic oxide, in contrast to the unchanged
property in 1M KOH.

It has been suggested by Kokhanov et al [32] and Shembel'
et al [33] that oxygen atoms can be incorporated into the bulk
of the oxide during the anodic evolution of oxygen in acidic
solutions.   Then the oxygen content in the oxide of the
anodized electrode was examined to clarify its connection with
the variation of the electrode characteristics.   In this exper-
iment, the oxidative power, ie the content of the active oxygen,
was determined [48], instead of the absolute value of the oxygen
content in the oxide.   The results are shown in Table 1.
Evidently the oxygen content in the oxide increases by the
anodic polarization in 0.5M H$_2$SO$_4$.   Therefore, it seems most
likely that the increase in the oxygen overpotential and the
decrease in the mechanical strength with the anodic polarization,

Table 1. Active oxygen content in Pt/MnOx
(value of δ in $MnO_{1+\delta}$)

| | Anodized for 20h | |
Non-anodized	0.5M H_2SO_4	1M KOH
0.53	0.81 (1mA/cm²)	0.52 (1mA/cm²)
	0.75 (10mA/cm²)	0.54 (10mA/cm²)

only in acidic solutions, are associated with the increase in
the oxygen content in the oxide. It has been reported that the
electronic conductivity of MnO_2 increases with the increasing
vacancy of oxygen [33]. Consequently, it is conceivable that
the overvoltage rises with the increasing resistivity of the
oxide due to an increase in the oxygen content and that the
mechanical strength is reduced by the distortion of the crystal
lattice due to the penetration of oxygen atoms.

The current-potential curves in the neutral solutions are
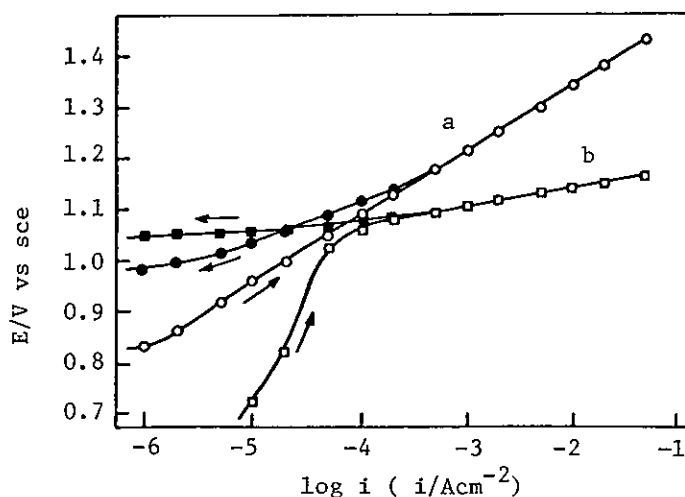shown in Figs. 6 and 7. The oxygen overvoltage in 0.5M K_2SO_4

Fig. 6. Current-potential curves of Pt/MnOx in neutral
solutions
a: in 0.5M K_2SO_4, b: in 1M KCl.
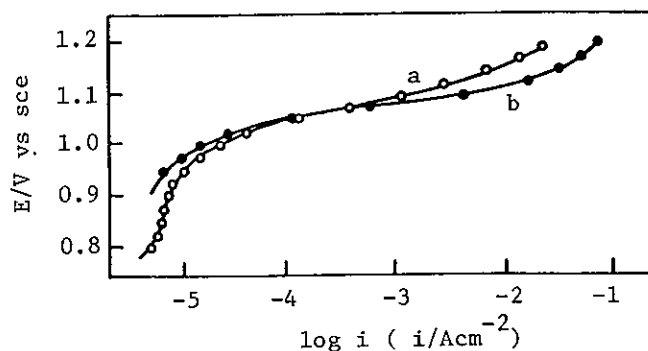
Fig. 7. Current-potential curves in 5M NaCl.
a: Ti/RuOx/MnOx, b: Pt/MnOx.
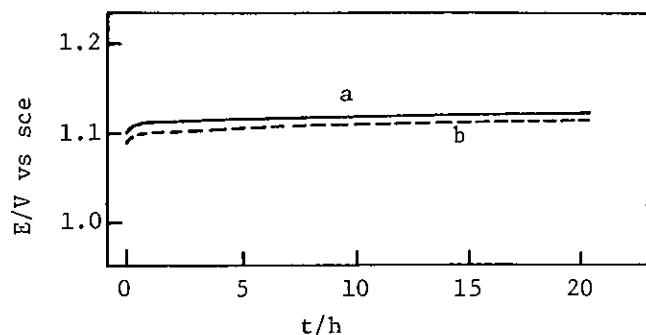
Fig. 8. Potential-time curves under anodic
polarization at $10mA/cm^2$ in 5M NaCl.
a: Ti/RuOx/MnOx, b: Pt/MnOx.

is rather higher than that in 0.5M H_2SO_4. Figure 8 shows the
potential-time curves under anodic polarization at $10mA/cm^2$.
Even in solutions containing chloride ions, the electrodes remain
quite stable under the anodic polarization, and chlorine evolves
with low overvoltage. Hence it may be concluded that the
Pt/MnOx and Ti/RuOx/MnOx are active catalysts for the chlorine
evolution reaction.

2. Oxygen evolution reaction

Figures 9 and 10 show the galvanostatic polarization curves on the Pt/MnOx electrode in 0.5M H_2SO_4 and 1M KOH, respectively. From both figures, Tafel lines with the slope of 0.11V were obtained after the correction of the iR drop in the region of the high current density. The polarization curves were galvanostatically measured in the various solutions with different activities of OH^- ion prepared by diluting the original
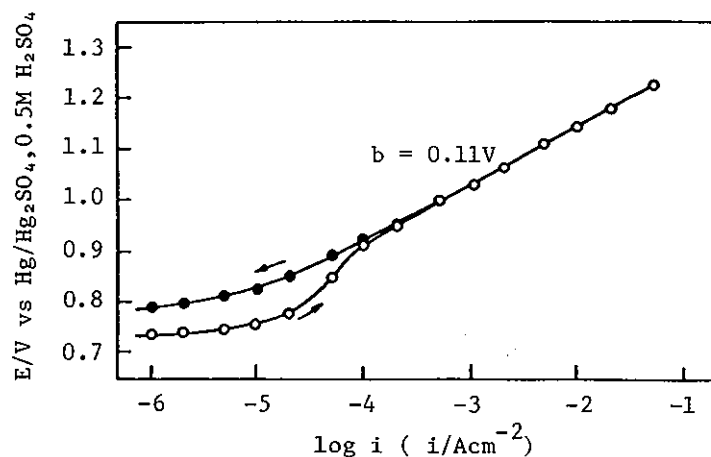
Fig. 9. Current-potential curve of Pt/MnOx in 0.5M H_2SO_4.
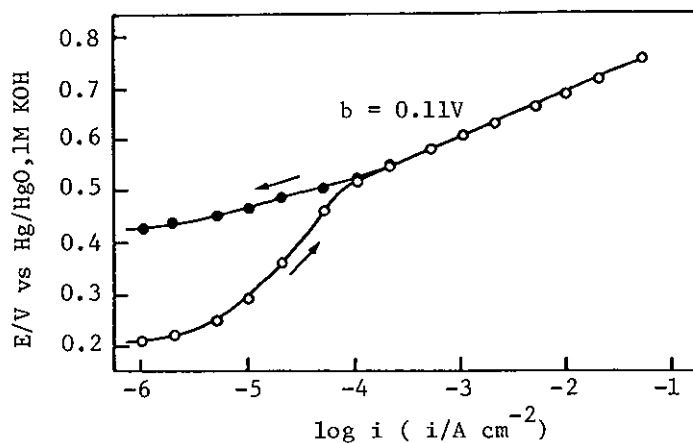
Fig. 10. Current-potential curve of Pt/MnOx in 1M KOH.

- 16 -
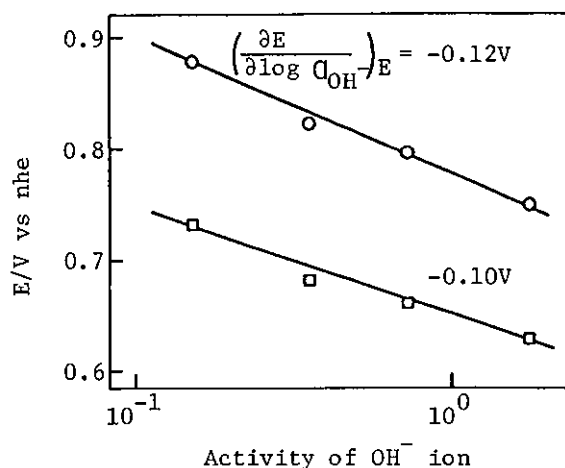
Fig. 11. Activity ($a_{OH}-$) dependence of anodic
potential at constant current density
in KOH solutions.

o : i = 5mA/cm², □ : i = 0.2mA/cm².
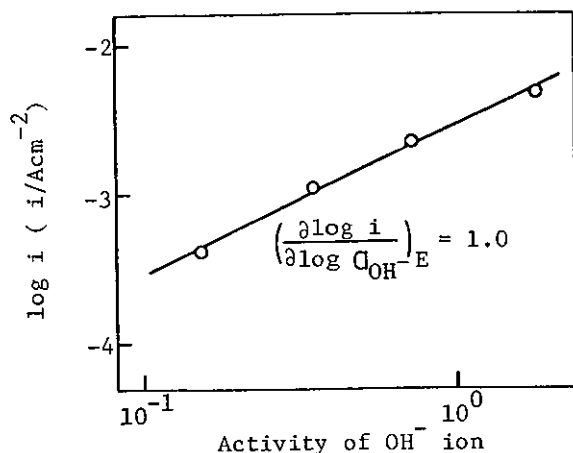
Fig. 12. Activity ($a_{OH}-$) dependence of current
density at constant potential (E=0.75V vs nhe).

solution of 2M KOH with twice-distilled water.   From these

polarization curves on the Pt/MnOx electrode, the anodic po-

tentials at constant current density are plotted in Fig. 11 as

a function of OH⁻ ion activity by using the activity data of

KOH solution [49].   The activity dependence of current density

at the fixed potential is shown in Fig. 12. Such measurements
were carried out also in the acidic solutions prepared by mixing
the original solution of 0.5M H_2SO_4 and 0.5M K_2SO_4 in various
ratios.

The kinetic parameters obtained from the above measurements
are summarized in Table 2. Consequently, the experimental
overall current density for the anodic evolution of oxygen can
be formulated as

$$i = nFk\exp(FE/2RT) \qquad (1)$$

in acidic solution and

$$i = nFk'a_{OH}-\exp(FE/2RT) \qquad (2)$$

in alkaline solution, where k and k' are the rate constants and
other symbols have their usual meanings.

Any one of the oxygen reaction paths already proposed by
Bockris [50] and Damjanovic et al [51] well satisfy the present
data if the first step, or

Table 2. Summary of observed diagnostic criteria

	b	Acidic solution $\left(\dfrac{\partial E}{\partial \log a_{H^+}}\right)_i$	$\left(\dfrac{\partial \log i}{\partial \log a_{H^+}}\right)_E$
Experimental value	0.11V	0	0
Idealized value	2.3 x 2RT/F	0	0

	b	Alkaline solution $\left(\dfrac{\partial E}{\partial \log a_{OH^-}}\right)_i$	$\left(\dfrac{\partial \log i}{\partial \log a_{OH^-}}\right)_E$
Experimental value	0.11V	−0.11V	1.0
Idealized value	2.3 x 2RT/F	−2.3 x 2RT/F	1

$$S + H_2O \rightarrow S\text{-}OH + H^+ + e \qquad (3)$$

in acidic solution and

$$S + OH^- \rightarrow S\text{-}OH + e \qquad (4)$$

in alkaline solution are rate determining, where S stands for
a site at the electrode surface. With an assumption such as
these first steps being rate-controlling, the current expression
in the Tafel region where the back reaction may be ignored can
be written as

$$i = nFk_1 a_{H_2O} \exp(\beta FE/RT) \qquad (5)$$

in acidic solution and

$$i = nFk_1' a_{OH^-} \exp(\beta FE/RT) \qquad (6)$$

in alkaline solution, where k_1 and k_1' are the rate constants
for the first steps and β is the symmetry factor. The theo-
retically deduced rate equations (5) and (6) are consistent with
the experimentally obtained expressions (1) and (2), respectively
if the usual assumption of $\beta = 1/2$ and $k_1 a_{H_2O} = k$ are made.
It therefore concluded that the primary discharge step of an
H_2O molecule or OH^- ion, corresponding to acidic or alkaline
solution, is rate-determining in the anodic evolution of
oxygen on Pt/MnOx electrode.

The galvanostatic polarization curve obtained on the
Ti/RuOx/MnOx electrode in 1M KOH is shown in Fig. 13, compared
with that obtained on the Pt/MnOx electrode. The anodic
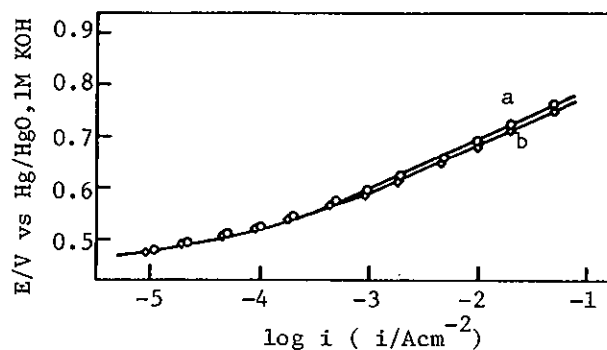Tafel slope of the curve on the Ti/RuOx/MnOx electrode is $b_a =$

Fig. 13. Current-potential curves in 1M KOH.
a: Pt/MnOx, b: Ti/RuOx/MnOx.

0.11V the value of which is agreement with that obtained on the
Pt/MnOx electrode.   From the Tafel slope and other parameters
for the oxygen evolution reaction, it is concluded that the
oxygen evolution reaction on the Ti/RuOx/MnOx electrode in 1M
KOH is also controlled by the step of the primary OH^- ion dis-
charge, or equation (4).   On the other hand, the value of b_a
for the oxygen evolution reaction on the Ti/RuOx electrode in
1M KOH has been determined to be 0.04V [24].   Therefore, this
difference in value of the Tafel slope supports the preceding
discussion that the MnOx acts as the electrode catalyst for the
anodic reaction on the Ti/RuOx/MnOx electrode.   This means that
the anodic evolution of oxygen takes place on the surface of the
Mn oxide.

Typical Arrhenius plots at constant overvoltage for the
oxygen evolution reaction on the Ti/RuOx/MnOx and Pt/MnOx
electrodes in 0.5M H_2SO_4 and 1M KOH are shown in Fig. 14.   An
apparent activation energy can be calculated from the gradient
of each straight line by using equation (7) [51,52],
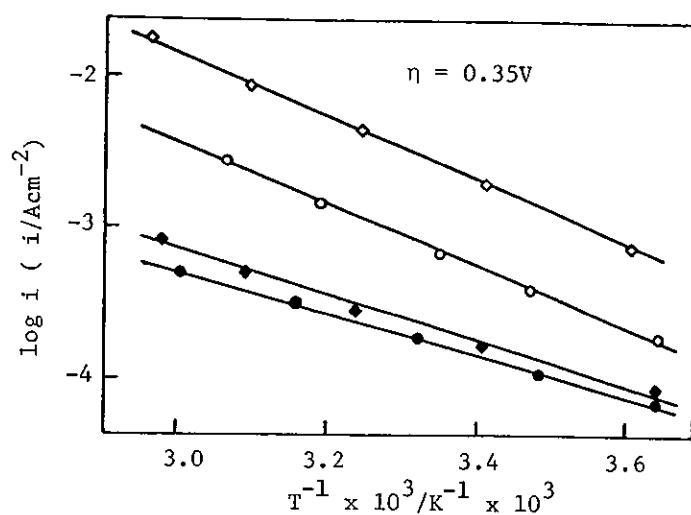
Fig. 14. Typical Arrhenius plots for O_2 evolution
in 1M KOH (open symbols) and in 0.5M
H_2SO_4 (closed symbols).
o,●: Pt/MnOx, ◇,◆: Ti/RuOx/MnOx.

Table 3. Apparent activation energy for the oxygen
evolution reaction

	ΔH (kJ·mol^{-1})			
	Ti/RuOx/MnOx		Pt/MnOx	
overvoltage η (V)	0.5M H_2SO_4	1M KOH	0.5M H_2SO_4	1M KOH
0.25		60.2		72.7
0.35	46.0	56.8	60.6	59.4
0.45	43.9	56.4	62.3	56.9

$$\Delta H^{\ddagger}(\eta) = -2.303R(\partial \log i / \partial (1/T))_{\eta} + \alpha nF\eta \quad [cal/mole] \quad (7)$$

where $\alpha n = 2.303RT/bF$, and F is a Faraday constant. Activation
energies for the oxygen evolution reaction calculated from
Arrhenius plots are summarized in Table 3. The substantial
identity of the activation energy between on the Pt/MnOx and
the Ti/RuOx/MnOx electrode is in accord with the prior results

that the mechanism of the oxygen evolution reaction on the Ti/RuOx/MnOx electrode is the same as that on the Pt/MnOx electrode. Furthermore, the values in Table 3 are also consistent with those on the bright Pt [50] and the Pt oxide [44] electrodes where the step of the primary OH^- ion discharge is rate-determining process in the oxygen evolution reaction, in agreement with the case on the Mn oxide electrodes.

The relative catalytic activity was evaluated for the oxygen evolution reaction. Roughness factors of the three kinds of electrodes under studying are summarized in Table 4. Each of roughness factor is defined as a value obtained by dividing the electrochemically working area by the apparent one. The working area can be estimated by measuring the amount of adsorption of Zn^{++} ion [40]. Considering the accuracy of the measurement of adsorption quantity, the measurement of which was carried out more than four times for each kind of electrodes, these roughness factors are regarded as the same magnitude. Furthermore, these values are comparable to that measured for DSA (Ti/RuOx) [24], and it may be, therefore, concluded that such roughness factors are one of the characteristics of the oxide electrodes prepared by the thermal decomposition in this manner. From the results in Table 4, the catalytic activity of

Table 4. Roughness factors of test electrodes

Electrode	Roughness factor
Ti/MnOx	50 – 70
Pt/MnOx	50 – 100
Ti/RuOx/MnOx	60 – 80
Ti/RuOx *	60 – 80

* Reference[24]
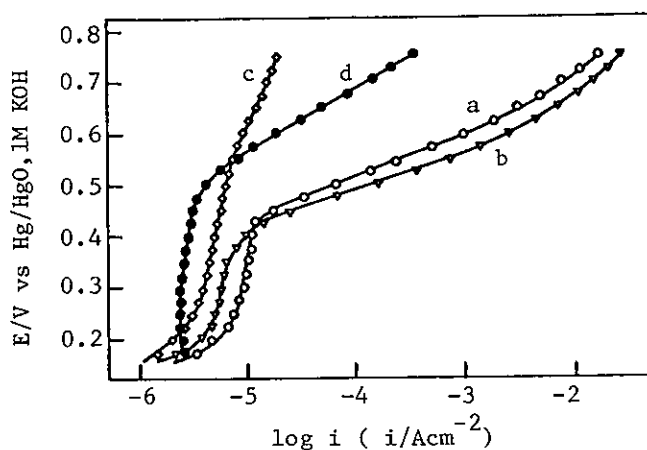
Fig. 15. Current-potential curves in 1M KOH.
a: Pt/MnOx, b: Ti/RuOx/MnOx, c: Ti/MnOx,
d: Pt.

each electrode is able to be compared by employing the apparent
current density.   The anodic polarization curves obtained on
the Ti/MnOx, Pt/MnOx and Ti/RuOx/MnOx electrodes are shown in
Fig. 15, compared with that obtained on the bright Pt electrode.
Since the roughness factor of the bright Pt electrode is esti-
mated to be more or less approximately 10, the current densities
on the Pt/MnOx and Ti/RuOx/MnOx electrodes are high by 100 times
or more, compared to that on the bright Pt electrode at the
potential of 0.7V (vs Hg/HgO, 1M KOH).   It is, therefore,
apparent that the catalytic activity of the Mn oxide is much
superior to that of the platinum for the anodic evolution of
oxygen.

In Table 5, the oxygen overvoltage for the Ti/RuOx/MnOx
electrode developed in this work is compared with those for the
anode materials so far used industrially.   The comparison may
be made for the overvoltage at $10mA/cm^2$ and $100mA/cm^2$ in apparent

Table 5. Oxygen overvoltages for various anodes in 1M KOH

Anode material	Overvoltages (V)	
	$0.01 Acm^{-2}$	$0.1 Acm^{-2}$
Platinum *	1.32	1.50-1.56
Platinized platinum *	0.66	0.89-0.90
Graphite *	0.96-0.98	1.12-1.17
Nickel *	0.75-0.76	0.91-0.93
Lead *	0.97	1.02-1.04
DSA (RuOx) **	0.22	0.27
DSA (IrOx) ***	0.28	0.32
Ti/RuOx/MnOx	0.40	0.51

*   Reference[53]
**   Reference[24]
*** Reference[26]

current density.   The overvoltage for the Ti/RuOx/MnOx electrode
is higher by 100 - 200mV than that for DSA being developed
recently, but much lower than those for the other conventional
anode materials such as graphite and nickel.

Though Mn oxide is somewhat inferior to Ru oxide and Ir
oxide in the catalytic activity, the material of the Mn oxide
electrode is abundantly present and inexpensive.   Therefore,
it may be expected that Mn oxide can practically be used as an
anode in some electrolysis industries.

4.   SUMMARY

The anodic characteristics of the film-type manganese oxide
(MnOx) electrodes, prepared by thermal decomposition of manganese

nitrate solution, were studied in aqueous solutions.   The
results obtained in this chapter are summarized as follows.

1. The Ti/MnOx electrode had a high resistivity due to
a thick TiO_2 film, despite strong adhesion between the oxide
film and the Ti substrate.

2. The anodic characteristics were improved by replacing
Ti with Pt or RuOx-coated Ti as a substrate.   That is, the
Pt/MnOx and Ti/RuOx/MnOx electrodes showed good anodic charac-
teristics with a relatively low overvoltage for oxygen evolution.

3. On the MnOx film electrodes, the primary water or hy-
droxide ion discharge step is rate-determining in the anodic
evolution of oxygen.

4. Evaluation of the catalytic activity showed that the
MnOx is among the most active materials for anodic evolution of
oxygen, except for some noble metal oxides, and that the Ti/RuOx/
MnOx electrode would be useful for water electrolysis.

CHAPTER 2

THE ANODIC CHARACTERISTICS OF MASSIVE MANGANESE OXIDE
ELECTRODES

1.   INTRODUCTION

In chapter 1, it was suggested that the manganese oxide
film electrodes prepared by the thermal decomposition method
act as an effective catalyst for the anodic evolution of oxygen
and chlorine.   However, this type of electrode revealed the
different characteristics depending on the kind of substrate
materials.   Therefore, in this chapter, the massive manganese
oxide was synthesized and its anodic polarization characteristics
were investigated for the purpose of eliminating the various
factors influenced by substrates.

No electrochemical study of massive manganese oxides has
been carried out except for the recent work by Naumann et al [54],
in which the $\beta-MnO_2$ was regarded as a degenerated n-type semi-
conductor in the aqueous solution systems despite of the
electrode reaction of the oxide itself.   In the present work,
the anodic polarization behaviours of the $\beta-MnO_2$ and the re-
lating manganese oxide were investigated over the wide potential
region.   And then, the relationship between the electrochemical
properties and the oxide compositions of the manganese oxide
anodes were clarified.

2. EXPERIMENTAL

1. Preparation of test electrodes

The preparative procedure of the massive manganese dioxide was almost the same as that reported by Wiley and Knight [55]. A portion of 1.0ml $Mn(NO_3)_2$ aqueous solution (50vol.%) was introduced in the test tube of 10mm diameter, and thermally decomposed at $170 \pm 10°C$ in air. After cooling, the additional 1.0ml $Mn(NO_3)_2$ solution was applied to the decomposed product in the bottom of test tube and then decomposed in the same condition. By repeating these procedures 5 times, about 5g of the massive product was obtained. The sample was taken out from the test tube and held in the electric furnace at $170 \pm 2°C$ for about 20h, in order to completion of the thermal decomposition. By polishing with emery papers, the tablet-shape oxide of 9mm diameter and about 2mm thickness was prepared.

The tablets were then thermally treated at various temperatures for 6 - 20h. The resulting samples were appreciably porous so that the waterproof treatment was performed for the tablets by impregnating with polystyrene resin dissolved in benzene solvent. Both planes of tablet were polished again, and a Pt wire lead was then connected to the one side of tablet with silver paste. The other side was exposed to solution as the test plane, the remainder masked off by an insulating resin.

2. X-ray and chemical analyses

The oxide composition of the thermally treated tablets were determined by the X-ray diffraction method. The

Table 6. Test electrodes

	Heat treatment		X-ray analysis	Chemical analysis (O/Mn)	Specific resistance (Ωcm)	Classification
	Temp.(°C)	Time(h)				
1	Non-treated		β-MnO$_2$	2.00	0.12	A
2	460	20	β-MnO$_2$	2.00	—	A
3	470	20	β-MnO$_2$	—	—	A
4	480	6	β-MnO$_2$	—	—	A
5	480	20	β-MnO$_2$ + α-Mn$_2$O$_3$	1.97	1.1	B
6	490	20	β-MnO$_2$ + α-Mn$_2$O$_3$	1.62	1.7-3.0	B'
7	500	20	α-Mn$_2$O$_3$	1.61	5.3-8.0	C

diffraction pattern of the oxide without the heat treatment showed that of the β-MnO$_2$. In addition, the chemical analysis was carried out by the iodide method reported by Kang et al [48].

The results of these analyses were shown in Table 6, together with the sepecific resistances measured by the four-probe method. The temperatures were controlled within an error of $\pm 2°C$. The chemical compositions of the test electrodes heated below 470°C are the same as that of non-treated one, and those oxides are composed of polycrystal β-MnO$_2$. The values of the specific resistance are in reasonable agreement with that reported previously [55,56]. By the heat treatment above 480°C, a part of β-MnO$_2$ is decomposed to form the mixed oxide with α-Mn$_2$O$_3$. However, the heat treatment to more extent is necessary for the complete change in composition because of the voluminousness of the sample. The most of β-MnO$_2$ changes to α-Mn$_2$O$_3$ by heat-treating at 500°C for 20h. Based on the oxide composition, hereinafter, these electrodes are conveniently divided into four groups; A, B, B' and C as shown in the table.

3. Electrochemical measurements

The polarization characteristics of the test electrodes
were measured in aqueous solution of 0.5M H_2SO_4, 0.5M K_2SO_4,
1M HCl, 1M KOH, 3M NaCl and 2M KBr at 30°C, and the mixed
solutions of two kinds of electrolyte were used for the de-
termination of the reaction order.   The reference electrode
was a hydrogen electrode (he) in the same solution or a saturated
calomel electrode (sce).   The other experimental procedures
were same as those described in the previous chapter.

3.   RESULTS AND DISCUSSION

1. Diffusion process of proton in the massive Mn oxides

The typical cyclic voltammograms in 0.5M H_2SO_4 are shown
in Fig. 16, where (A) and (B) indicate the electrodes without
the heat treatment and with the treatment at 480°C for 20h,
respectively.   The large capacitance-like currents appeared
over the whole potential region in Fig. 16 is the characteristic
behaviour for the manganese dioxide electrode.   Such voltammo-
grams were also observed for the RuO_2 and IrO_2 electrodes
prepared by the thermal decomposition method [26, 57].

The current densities of the anodic peaks at approximately
1.5V vs he in the electrode A and B were dependent on the rate
of the potential sweep and independent on the stirring of the
electrolytes.   The plots of the peak current densities, i_p,
against the square root of the sweep rate, $v^{1/2}$, are straight
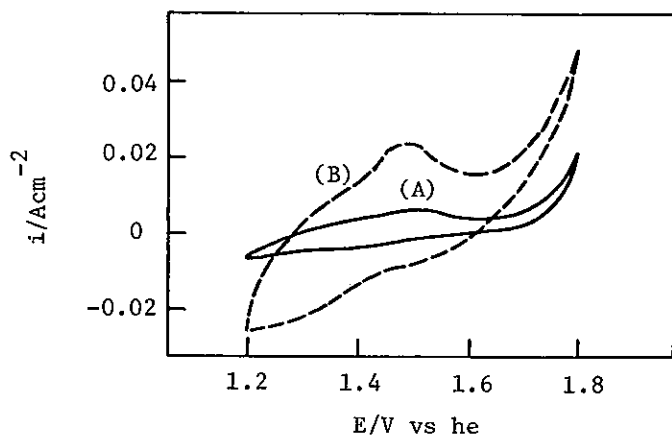line, as shown in Fig. 17.   These linear relations follow the

Fig. 16.   Cyclic voltammograms of massive Mn oxides
in 0.5M H_2SO_4.
(A): non treated, (B): heat treated at
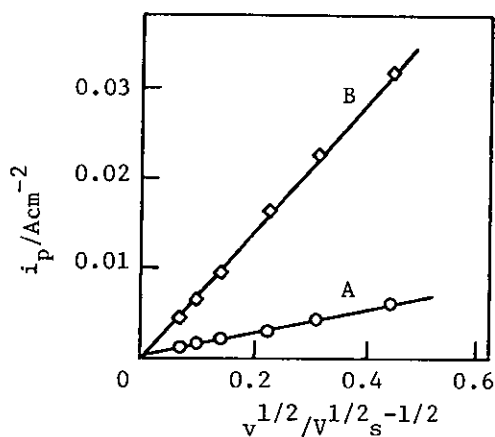480°C for 20h.   Sweep rate: $0.1Vs^{-1}$.

Fig. 17. i_p vs $v^{1/2}$ plots obtained from
cyclic voltammograms.
A: electrode A, B: electrode B

theoretical equation derived from the assumption of the linear
diffusion for reactant in the solution [58],

$$i_p = k_1 C^\circ D^{1/2} v^{1/2} \ , \tag{8}$$

where C° and D are the bulk concentration and the diffusion

- 30 -

coefficient of the reactant, respectively, and k_1 is the proportionality constant.

On the other hand, when the constant anodic current was applied to these electrodes, the potentials were changed in such a manner as

$$E = E_r + k_2 t^{1/2} \ , \tag{9}$$

where E_r and k_2 are the rest potential of the electrode and the proportionality constant, respectively. The E-$t^{1/2}$ plots at the various anodic currents are shown in Fig. 18 for electrode B. Such changes in potentials are explained by the theoretical equation (10) [59],
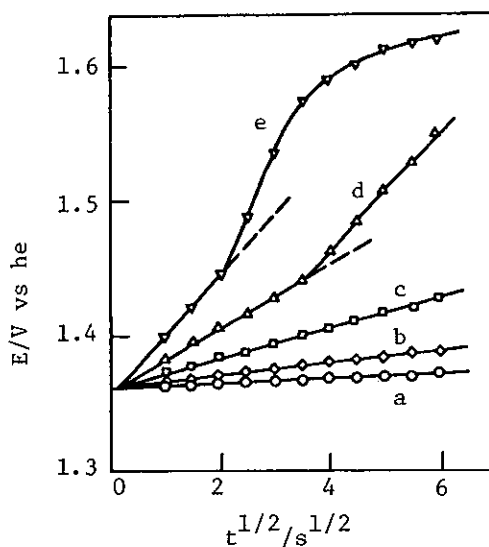

Fig. 18. Potential-time curves at constant
currents in 0.5M H_2SO_4 for
electrode B (S = 0.64cm^2).
a: at 0.05mA, b: 0.1, c: 0.2,
d: 0.5, e: 1.0.

$$\eta = E - E_0 = \frac{RT}{nF}\frac{i}{A}[\frac{2t^{1/2}}{nF\pi^{1/2}}(\frac{1}{C_x^\circ D_x^{1/2}} + \frac{1}{C_y^\circ D_y^{1/2}}) + \frac{1}{i_\circ}] \ , \quad (10)$$

where the subscripts x and y indicate the oxidized and reduced species, respectively, and other symbols have their usual meanings.

Strictly speaking, the equations (8) and (10) are valid for reaction in the solution, but the results shown in Figs. 17 and 18 suggest that the reaction involving the diffusion process in the solid seems to follow those equations because the oxidation of Mn oxides proceeds in homogeneous solid phase [31]. It is also suggested that the anodic currents under the relatively low polarization of Mn oxide electrodes are attributed to the diffusion process of H^+ ions in the oxides. The H^+ ions in the Mn oxides, produced by the attachment of the combined water to the manganese (III) oxides, is considered to participate in the following reaction

$$MnOOH \rightarrow MnO_2 + H^+ + e \ . \quad\quad\quad (11)$$

This is the reverse reaction of the first step in the cathodic discharge processes in the general form [31].

From equation (10), one obtains

$$d\eta/dt^{1/2} = \frac{2RTi}{(nF)^2\pi^{1/2}A}(\frac{1}{C_x^\circ D_x^{1/2}} + \frac{1}{C_y^\circ D_y^{1/2}}) \ . \quad (12)$$

Hence, the value of $(1/C_x^\circ D_x^{1/2} + 1/C_y^\circ D_y^{1/2})$ can be estimated from the slopes of the straight lines shown in Fig. 18. Figure 19 shows the $d\eta/dt^{1/2} - i$ relation for the electrode A and B. From their slopes and the relation,
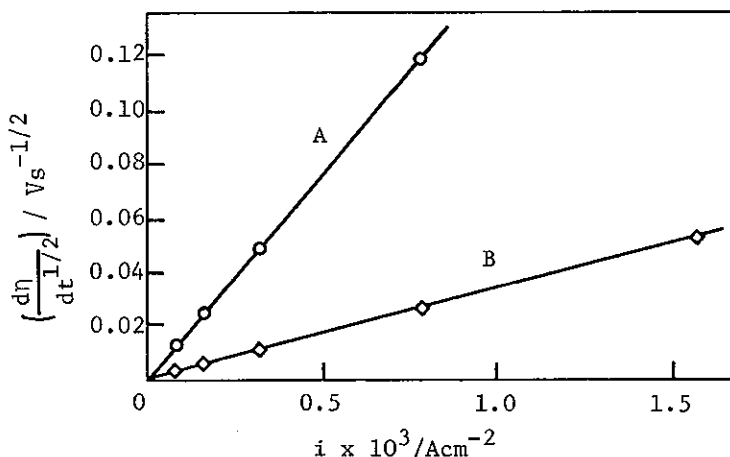
Fig. 19. $d\eta/dt^{1/2}$ vs i plots obtained from potential-
time curves.

A: electrode A, B: electrode B.

$$1/C_x^\circ D_x^{1/2} \ll 1/C_y^\circ D_y^{1/2} \qquad\qquad (13)$$

x: H^+ in electrolyte

y: H^+ in electrode (MnOOH),

the value of $C_H^\circ D_H^{1/2}$ in the oxide are calculated to be 5.05 x 10^{-8} for electrode A and 1.11 x 10^{-8} mole $cm^{-2}s^{-1/2}$ for electrode B. As the concentration of MnOOH in the bulk of the manganese dioxide is regarded as 10^{-3} - 10^{-4} mole cm^{-3} [39,60], the diffusion coefficient of H^+ ion, D_{H^+}, in the manganese dioxide is estimated to be 10^{-8} - 10^{-10} cm^2 s^{-1}. This value of D_{H^+} is in substantial agreement with that reported by Larange and Brenet for the polycrystalline γ-MnO_2 (8 x 10^{-8} cm^2 s^{-1}) [61], whereas it is considerably higher than that obtained by Scott for the powdered γ-MnO_2 (1.2 x 10^{-18} cm^2 s^{-1}) [62]. Furthermore, the quantity of electricity consumed during the anodic charging is calculated to be about 10mC cm^{-2}, which

corresponds to the charging in the several ten layers of the oxide electrode. These experimental results consequently suggest that these Mn oxides are easily oxidized and reduced, accompanied by the transfer of the H^+ ion in the layers near the surface.

2. Anodic evolutions of oxygen and chlorine on massive Mn oxide

The potentiostatic polarization curves in 0.5M H_2SO_4 are shown in Fig. 20. The measurements were carried out with the direction from more anodic potential to lower one, and the majority of the observed currents were assigned to the anodic evolution of oxygen. It is evident that α-Mn_2O_3 contributes to the activity for the oxygen evolution reaction, since the current density on electrode B is higher by one order of magnitude or more than that on electrode A at the same potential.
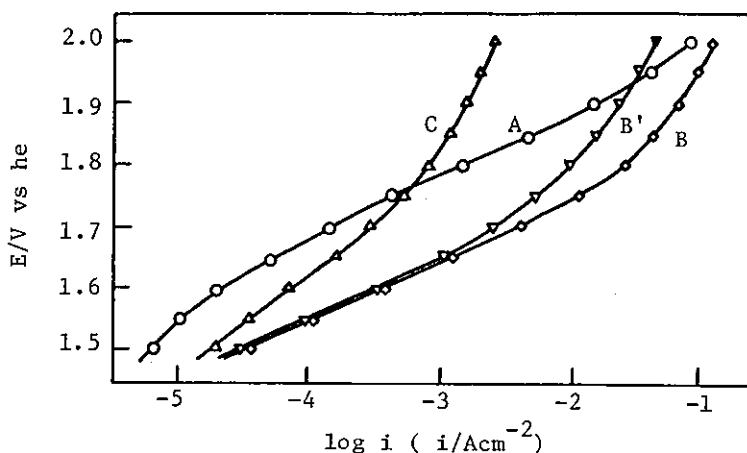

Fig. 20. Potentiostatic current–potential curves in 0.5M H_2SO_4.
A: non-treated, B: heat treated at 480°C for 20h,
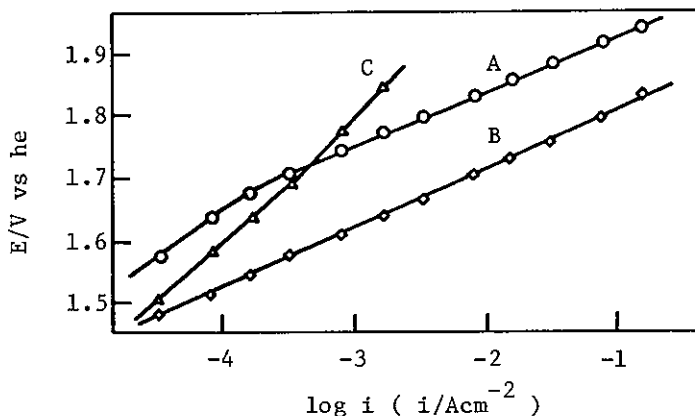B': at 490°C for 20h, C: at 500°C for 20h.

Fig. 21. Galvanostatic current-potential curves in 0.5M H₂SO₄.
A: electrode A, B: electrode B, C: electrode C.

Comparing the polarization curve of the electrode B with those
of electrode B' (heat-treated at 490°C) and electrode C (heat-
treated at 500°C), it is apparent that the thermal treatment at
higher temperature causes the decrease of the current density.
This phenomenon is due to the ohmic loss in the oxides, since
the contents of α-Mn$_2$O$_3$, and then the electric resistivities,
increase with the elevation of temperature in thermal treatment.
Figure 21 shows the galvanostatic polarization curves in which
iR correction were made for electrodes A, B and C in 0.5M H$_2$SO$_4$.
The same value, 0.11V, of the Tafel slopes are obtained for both
electrodes A and B, which coincides with the value for the film-
type electrodes, Pt/MnOx and Ti/RuOx/MnOx, in chapter 1.

The degree of the anodic dissolution of the test electrodes
were extremely small as a whole, but a clear difference was
detected between the rates of the dissolution reactions for
electrodes A and B.   The current efficiencies of the anodic
dissolutions for the three kinds of electrodes were measured at

- 35 -

Table 7. Current efficiency for anodic dissolution
of the massive electrodes in 0.5M H_2SO_4.

Current	Current efficiency * (%)		
$(mA/0.64cm^2)$	A	B	C
10	$<10^{-4}$	0.090	——
20	$<10^{-4}$	0.120	——
50	$<10^{-4}$	0.265	——
100	0.002	0.151	0.083

* For the reaction, $Mn(III) \rightarrow Mn(VII) + 4e$.

different current densities and are summarized in Table 7.   In
this case, the values were calculated from the dissolved quantity
determined, with the assumption of four-electron oxidation.
From the fact that the rate of dissolution of electrode A is
much smaller than that of electrode B, it is strongly suggested
that the anodic dissolution reaction proceeds at the Mn(III)
site of the electrode surface.   Furthermore, if the dissolution
takes place through the same intermediate as the oxygen evolution
on these Mn oxides, it may be considered that the Mn(III) site
is rather active more than the Mn(IV) site for the anodic evo-
lution of oxygen.

The iR-corrected polarization curves in 1M KOH and 3M NaCl
solutions are shown in Figs. 22 and 23, respectively.   The
shape of the curves in Fig. 22 is similar to that obtained on
the film-type electrodes such as Pt/MnOx and Ti/RuOx/MnOx
electrodes.   For the reaction of chlorine evolution, however,
the massive Mn oxide electrodes revealed the behaviour different
from the film-type electrodes (see Pt/MnOx in Fig. 23).

The chlorine evolution reaction in the acidic solution
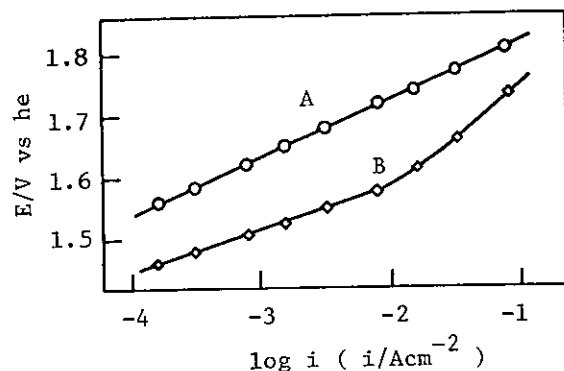
Fig. 22. Current-potential curves in 1M KOH.
A: electrode A, B: electrode B.
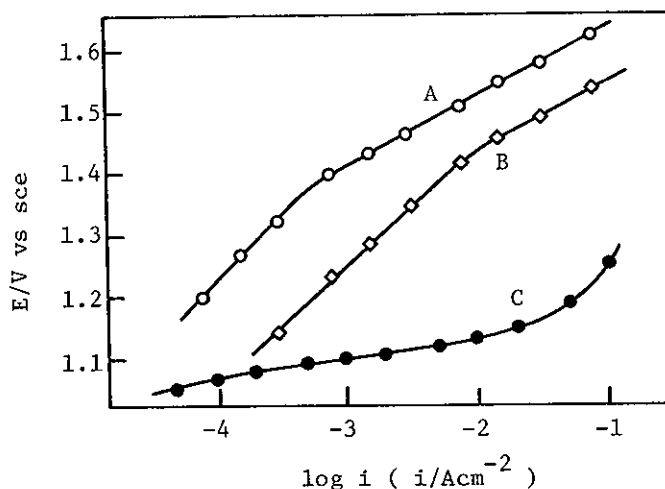
Fig. 23. Current-potential curves in 3M NaCl.
A: electrode A, B: electrode B, C: Pt/MnOx.

containing 3M NaCl was compared with the anodic oxidation of
bromide ion on the massive Mn oxide electrodes.   Figure 24
shows the polarization curves for the chlorine evolution together
with those for the oxygen evolution.   The chlorine evolution
reaction was experimentally confirmed to be proceeding with the
current efficiency of approximately 100% on each electrode in
the mixed solution of 3M NaCl and 0.5M H_2SO_4.   But, the

Fig. 24. Current-potential curves in 3M NaCl + 0.5M H_2SO_4
(closed symbols) and 0.5M H_2SO_4 (open symbols).
o,● : electrode A, ◇,◆ : electrode B.

polarization curve of electrode B for the chlorine evolution is

agreement with that for the oxygen evolution, and the somewhat

similar result was obtained for electrode A.   In the case of
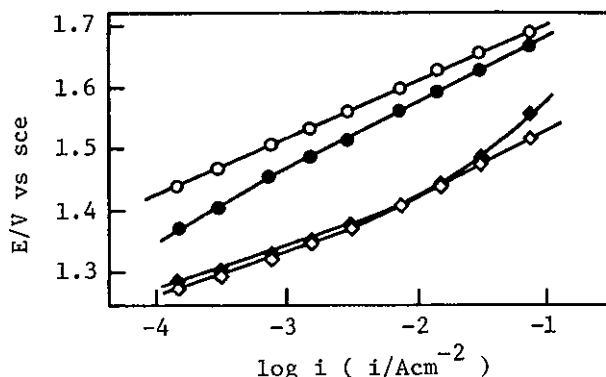
the latter electrode, the composition of the oxide, shown in

Table 6, is reflected on the polarization curve.   It is,

therefore, considered that the rate-determining step in the

chlorine evolution reaction is actually identical with that in

the oxygen evolution reaction on the massive Mn oxide electrodes.

This means the process of oxygen and chlorine evolution through

a common stage.   For the oxidation of bromide ion, however, the

Mn oxide electrodes exhibit the normal behaviour observed on

metal electrodes [63], as shown in Fig. 25.   This difference

in anodic behaviour seems to result from the redox potentials

of Cl^-/Cl_2 and Br^-/Br_2.   Bromide ion adsorbs on the surface of

the Mn oxides and then discharges with the normal mechanism,

whereas the charge transfer from chloride ion can occur only

after the oxidation of the electrode surface because the
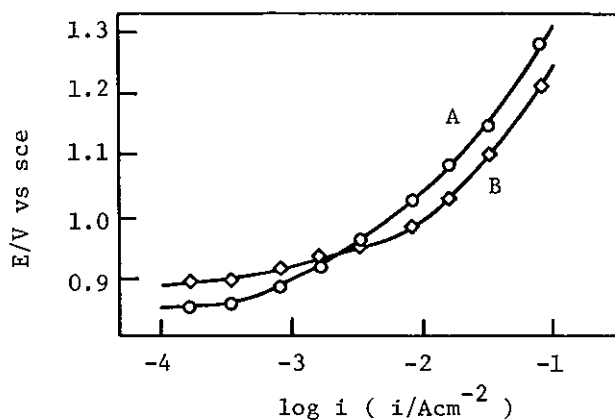
Fig. 25. Current-potential curves in 2M KBr + 0.5M H₂SO₄.
A: electrode A, B: electrode B.

oxidation potential of chloride ion seems to be higher than that of the electrode surface itself.

In order to support the above speculation, the reaction orders of various species were determined for oxygen and chlorine evolution reactions on the Mn oxide electrodes and the reaction mechanisms are discussed. The reaction orders were estimated by the dependency of the current densities at constant potentials on the activities of the reactive species in the solution.

Table 8. Summary of reaction orders for O_2 and Cl_2 evolution.

Electrolyte		Reaction order ($\log i/ \log a_j$)		Reaction
		A	B	
H_2SO_4 + K_2SO_4	low η	0.1	1.0	
(j = H^+)	high η	0.1	0.1	O_2
KOH		0.9	0.9	
(j = OH^-)				
NaCl		0	0	
(j = Cl^-)				Cl_2
NaCl + HCl		0	0	
(j = H^+)				

The results are shown in Table 8 with respect to each electrode.
For the reaction of anodic oxygen evolution, the reaction orders
of H^+ ion in the acidic solution and OH^- ion in the alkaline
solution are approximately zero and unity, respectively, except
for the low overvoltage region on electrode B where the partic-
ipation of the cathodic process can not be ignored. These data
for oxygen evolution reaction are practically in agreement with
those on the film-type electrodes. On the other hand, unusual
data were obtained for the chlorine evolution reaction on the
massive Mn oxide electrodes. In general, the reaction order
with respect to Cl^- ion in the anodic evolution of chlorine is
1 or 2 on usual metal and metal oxide electrodes [7, 64], and
the current density is also dependent on the pH of the electro-
lyte, especially at metal oxide electrodes [18]. However, the
present results show that on the massive Mn oxide electrodes
the reaction rate of the anodic chlorine evolution is independent
on the activities of not only proton but also chloride ion.
Such results with respect to the reaction orders and the anodic
polarization characteristics provide the following suggestions;
Even in the anodic evolution of chlorine, the rate-controlling
step is the same one as in the oxygen evolution, which is
probably the first charge transfer step involving the H_2O mole-
cule or the OH^- ion.

According to the model of the metal oxide-solution interface
proposed by Ahmed and Maksimov [65], the surface of the Mn oxide
in the acidic solution is represented by the forms such as

$$\left[\ge Mn \underset{OH_2}{\overset{OH}{\diagup \diagdown}} OH_2 \right]^+$$
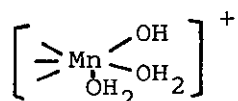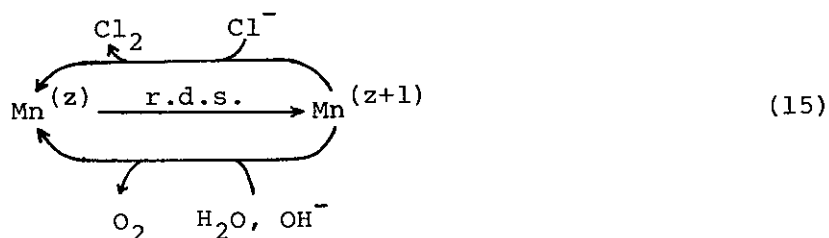
It is considered that the charge transfer process, or common rate-determining step both for oxygen and chlorine evolution, is expressed by the oxidation process of the central metal cation, $Mn^{(z)}$,

$$\left[\geqq Mn^{(z)} \overset{OH}{\underset{OH_2}{\overset{|}{-}}} OH_2 \right]^+ + H_2O \rightarrow \left[\geqq Mn^{(z+1)} \overset{OH}{\underset{OH_2}{\overset{|}{-}}} OH \right] + H_3O^+ + e \ , \quad (14)$$
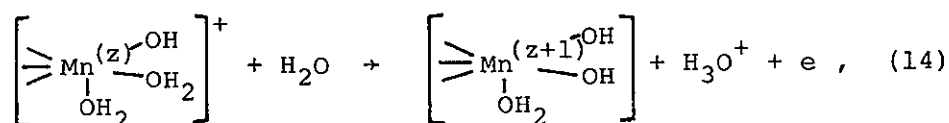
where z represents the valency of the manganese. Though the value of z is undefined, the active site is probably one formed from the Mn(III) for both reactions. Even on electrode A, whose bulk composition is β-MnO_2, the Mn(III) sites may be produced at the oxide surface by the formation of oxygen vacancy during the electrode preparation [66]. The high activity of the Mn(III) site may be similar to that of the Ir(III) site in the anodic oxide film of the Ir electrode reported by Gottesfeld and Srinivasan [67]. They have pointed out that high activities might be exhibited by metastable states of the oxide catalyst associated with intermediate oxidation states.

Although, in this work, no informations were obtained on the subsequent processes yielding finally O_2 and/or Cl_2 and re-generating the site $Mn^{(z)}$, one of the presumable following step is a catalytic cycle such as sheme (15), since the evolution reactions of both oxygen and chlorine take place via a common process.

$$
\begin{array}{c}
Cl_2 \quad\quad Cl^- \\
\nwarrow \quad\quad \nearrow \\
Mn^{(z)} \xrightarrow{\ r.d.s.\ } Mn^{(z+1)} \quad\quad (15) \\
\nwarrow \quad\quad \nearrow \\
\swarrow \quad\quad \searrow \\
O_2 \quad H_2O, \ OH^-
\end{array}
$$

Consequently, the H_2O molecule, the OH^- ion or the Cl^- ion may be oxidized to the oxygen and the chlorine, respectively, by the Mn in the high oxidation state, $Mn^{(z+1)}$, which is probably the Mn(IV) at the surface, and then the $Mn^{(z+1)}$ may be reduced to the initial low oxidation state, $Mn^{(z)}$. The somewhat similar mechanism with the valence change of oxide surface during the electrode reaction has been first proposed by Yeager et al [24] for the anodic evolution of oxygen on the DSA-type RuO_2 electrode in alkaline solutions and accepted by Srinivasan et al [68] for the same reaction on NiOx, $NiCo_2O_4$ and RuO_2/TiO_2 electrodes.

The reason for such unique characteristics of Mn oxide electrodes can be related to the high reactivities of Mn oxides and the redox potential of Mn(III)/Mn(IV) (E_o = 0.98V vs nhe for Mn_2O_3/MnO_2) which is fairly near those of Cl^-/Cl_2 and H_2O/O_2. Further details of the differences in the polarization characteristics between the massive Mn oxides and the film-type electrodes will be discussed in the next chapter.

4. SUMMARY

The anodic characteristics of the massive manganese oxides were investigated in aqueous solutions. The results obtained in this chapter are summarized as follows.

1. The thermal treatment of the massive $\beta-MnO_2$ at 480°C or above leads to the formation of $\alpha-Mn_2O_3$, and the redox reaction of Mn(III)/Mn(IV) accompanied by the diffusion of the H^+ ion

was characterized in the solid phase of the oxides.

2. The relatively high activity was observed for the anodic evolution of oxygen on the mixed oxide of $\beta\text{-MnO}_2$ and $\alpha\text{-Mn}_2\text{O}_3$, and the active site of the reaction was regarded as the Mn(III) site at the oxide surface.

3. It was suggested that the oxidation process of the Mn(III) site at the electrode surface is a common rate-determining step in both the oxygen and chlorine evolution on the massive manganese oxide electrodes.

CHAPTER 3

THE ANODIC CHARACTERISTICS OF THE MASSIVE β-MnO_2 DOPED
WITH NOBLE METALS IN SODIUM CHLORIDE SOLUTION

1.   INTRODUCTION

As shown in the previous chapter, the difference in charac-
teristics is observed for the anodic evolution of chlorine
between the massive manganese oxides and the film-type manganese
oxides.   It is most probable that incorporation of noble metals
into the manganese oxides occurs slightly in the film-type
electrodes, because the noble metals such as Ru and Pt are used
as an intermediate layer and a substrate, respectively.   Most
of noble metals and their oxides exhibit high catalytic activity
for the anodic evolution of chlorine [4-22].   Therefore, it
seems possible that the presence of small amounts of noble
metals in the massive manganese oxides affects their polarization
characteristics in NaCl solution.

In this chapter, in order to evaluate above supposition,
the massive manganese oxides were doped with a slight amount of
noble metals and then their anodic characteristics were investi-
gated mainly in 3M NaCl.   Furthermore, the role of doped metals
was discussed.

2. EXPERIMENTAL

The massive manganese oxides were prepared by the same procedure as that described in chapter 2. Foreign metals were doped in the massive manganese oxides by using mixed aqueous solution of 50vol.% $Mn(NO_3)_2$ and 0.1M chlorides of foreign metals (or metal salts) containing HCl as the original solutions for thermal decomposition. The temperature of the thermal decomposition was controlled at 160 – 180°C, and all of the resulting oxides were thermally treated at 450°C for 20h. The starting raw materials used and the predicted valences of the doped foreign metals are summarized in Table 9. To avoid complexity, the test electrodes of this type will be referred to as MnO_2-M(C), where C represents the concentration of the doped metal, M, in at.% M/Mn. The maximum concentration of the doped metals was fixed to 2at.%.

The X-ray diffraction patterns of all test electrodes exhibited that of pure β-MnO_2 and no patterns assigned to the metals or their oxides doped in β-MnO_2 were observed in any

Table 9. Summary of doped metals

Doped metal	Raw material	Predicted valency in β-MnO_2
Pd	$PdCl_2$	Pd(II) or Pd(0)
Pt	H_2PtCl_6	Pt(II) or Pt(0)
Ru	$RuCl_3$	Ru(IV)
Ir	$IrCl_4$	Ir(IV)
Rh	$RhCl_3$	Rh(III)
Ti	$TiCl_3$	Ti(IV)
V	NH_4VO_3	V(V)
Mn	$MnCl_2$	Mn(III)

cases.

Most of electrochemical measurements were performed in
aqueous solutions of 0.5M H_2SO_4 and 3M NaCl at 30°C.   The
electrolytic solutions were prepared from the special grade
reagents and twice-distilled water, and were purified by elec-
trolysis over 40h before use.   The current-potential curves
were galvanostatically measured under the conditions of N_2 gas
bubbling in electrolytic solutions in order to eliminate dis-
solved oxygen and to minimize the concentration overvoltages.
The ohmic drop was determined by the current interrupting
method.   The ac impedance measurements were carried out at
equilibrium potential in the Cl_2-saturated 3M NaCl solution
$(P_{Cl_2} = 1atm)$.

3.   RESULTS AND DISCUSSION

Figure 26 shows the current-potential curves obtained on
the MnO_2-Ru(0.5), MnO_2-Ru(1) and MnO_2-Ru(2) electrodes in 3M
NaCl, compared with those on the pure β-MnO_2 and Ti/RuOx/MnOx
electrodes.   At current densities higher than about $10mA/cm^2$,
slight bendings of the curves due to concentration polarization
are observed.   However, it was experimentally confirmed by
using rotating disk electrodes that high overvoltage observed
at the pure β-MnO_2 electrode cannot be attributed to concen-
tration overvoltage only.   The chlorine overvoltage as well as
the Tafel slope decreases with the increase in concentration of
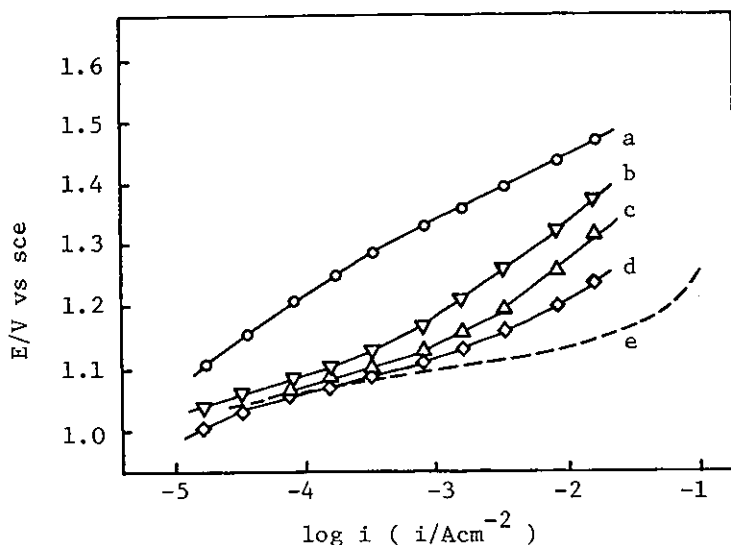doped Ru.   The curve of the film-type electrode, Ti/RuOx/MnOx,

Fig. 26. Current-potential curves of metal-doped
          electrodes in 3M NaCl.
          a:pure β-MnO$_2$, b:MnO$_2$-Ru(0.5), c:MnO$_2$-Ru(1),
          d:MnO$_2$-Ru(2), e:Ti/RuOx/MnOx.

is appreciably similar to that of the MnO$_2$-Ru(2) electrode:
such similarity may suggest that the RuOx used as an intermedi-
ate layer in the Ti/RuOx/MnOx electrode migrates in part to
the surface MnOx layer to form Ru-doped Mn oxide.

Figure 27 shows the current-potential curves of MnO$_2$
electrodes doped with 2at.% of different metals.   It is obvious
from this figure that Ru, Ir, Pt and Pd affect the chlorine
overvoltage in a striking manner.   Rh revealed little doping
effect and both Ti and V exhibited no effects on the chlorine
evolution reaction.   Furthermore, it is evident that chloride
ion contained in the original solutions for electrode preparation
is not responsible for the variation in anodic characteristics,
because the current-potential curve observed on the MnO$_2$-Mn(2)
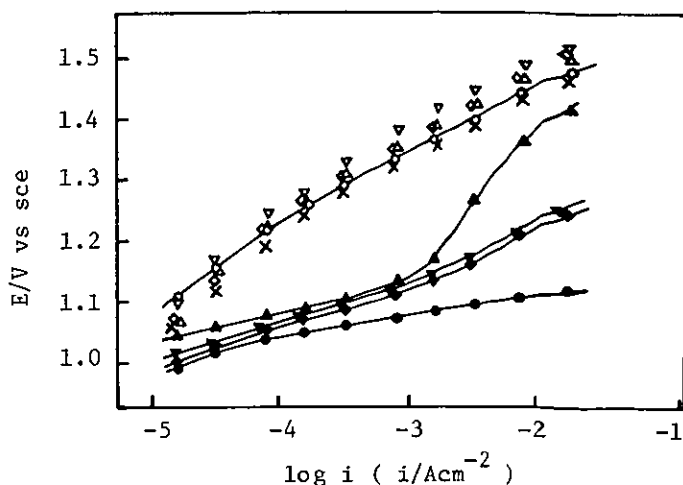electrode is approximately in agreement with the curve on the

Fig. 27. Current potential curves of metal-doped
          electrodes in 3M NaCl.
          o :pure β-MnO$_2$, X :MnO$_2$-Mn(2), $\triangle$:MnO$_2$-Ti(2)
          $\triangledown$:MnO$_2$-V(2), $\diamond$:MnO$_2$-Rh(2), $\blacktriangle$:MnO$_2$-Pt(2)
          $\blacktriangledown$:MnO$_2$-Ir(2), $\blacklozenge$:MnO$_2$-Ru(2), $\bullet$:MnO$_2$-Pd(2).

pure β-MnO$_2$ electrode.   Therefore, these doping effects may

reflect the catalytic activity for the chlorine evolution

reaction of the doped metals or their oxides.   The most ef-

fective dopant of all studied was Pd.   In fact, the Pd metal

or PdO possesses extremely high activity for the anodic evolution

of chlorine [69].

    In order to evaluate the doping effects on the oxygen

evolution reaction, the current-potential curves of various

electrodes were measured in 0.5M H$_2$SO$_4$, and the results are

shown in Fig. 28.   Any significant effects on the oxygen

evolution reaction were not observed on all electrodes examined.

Such difference in doping effects between the chlorine and

oxygen evolution reactions seems to be attributable to the

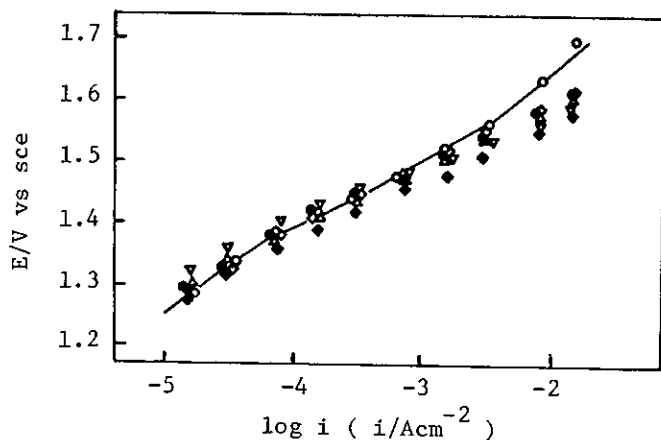difference in catalytic activities of β-MnO$_2$ itself for those

Fig. 28. Current-potential curves of metal-doped electrodes in 0.5M H_2SO_4.

○ : pure β-MnO_2, ● : MnO_2-Pd(2), ◇ : MnO_2-Ru(2)

◆ : MnO_2-Rh(2), △ : MnO_2-Ir(2), ▽ : MnO_2-Pt(2).

two reactions. For the oxygen evolution reaction, the catalytic activity of β-MnO_2 is as high as those of the doped metals. Therefore, the significant doping effects can not be revealed in the β-MnO_2 doped with the noble metals. On the other hand, the doped metals act effectively for the chlorine evolution reaction because of the relatively low activity of β-MnO_2 itself for that reaction.

Figure 29 shows variation of electrode potentials with time under the galvanostatic polarization at 5mA/cm^2 in 3M NaCl. The anodic shift of electrode potentials was observed at any electrodes within the first one hour, but it became negligible after that. Though the iR drops in the electrode potentials were corrected for the respective electrodes, the concentration overvoltages, which might be different in every electrode, are involved in the figure. Even after these experiments, the
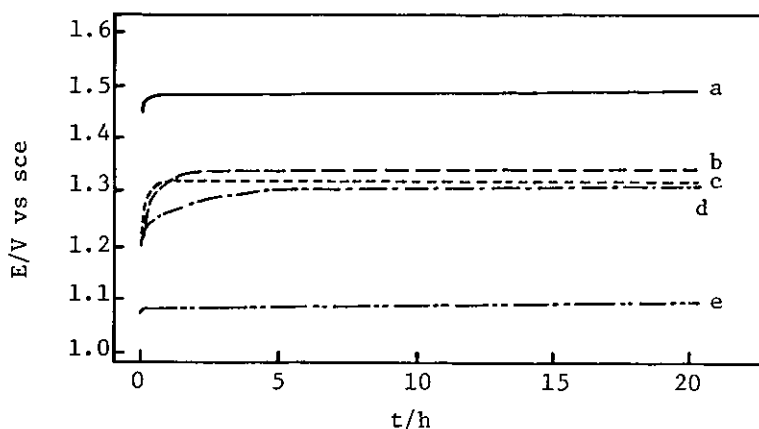
Fig. 29. Potential-time curves of metal-doped electrodes
at $5mA/cm^2$ in 3M NaCl.
a:pure β-MnO_2, b:MnO_2-Ir(2), c:MnO_2-Ru(2),
d:MnO_2-Pt(2), e:MnO_2-Pd(2).

current-potential curves could be well-reproduced for all

electrodes.   Furthermore, no changes of the electrode surfaces

were observed in their appearances.   These results suggest

that the anodic currents, shown in Fig. 27, are entirely due

to the anodic evolution of chlorine but not to the anodic dis-

solution of doped metals.

In order to elucidate the role of the doped metals, the

metal-adsorbed MnO_2 electrodes, MnO_2/M^x(ad), were prepared and

their polarization characteristics were measured in 3M NaCl

solution.   The adsorption of noble metals on the pure β-MnO_2

electrodes were performed by soaking the pure β-MnO_2 electrode

in 10^{-2}M solutions of noble metal chloride containing 2% HCl

for 50h, followed by washing with deionized water for 10min to

remove ions adhered physically on the oxide surface.   The

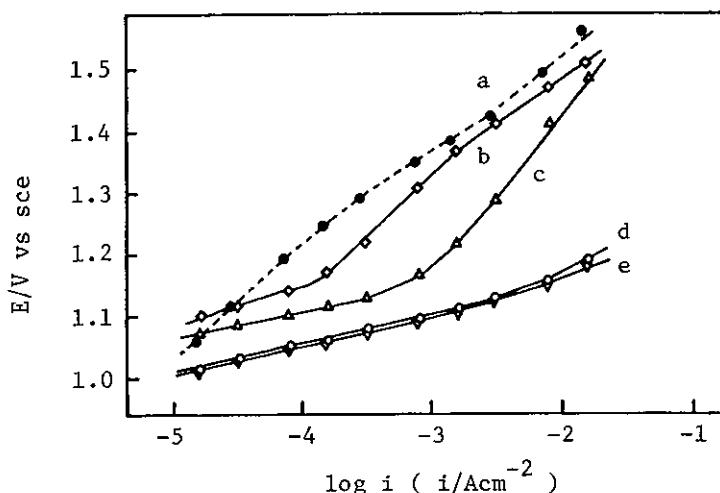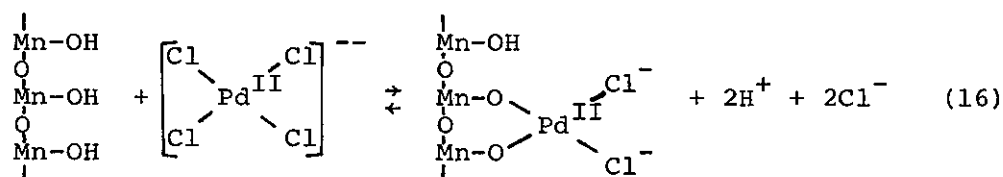current-potential curves on metal-adsorbed electrodes are shown

Fig. 30. Current-potential curves of metal-adsorbed
electrodes in 3M NaCl.
a:pure β-MnO$_2$, b:MnO$_2$/Rh^{III}(ad), c:MnO$_2$/Pt^{IV}(ad),
d:MnO$_2$/Pd^{II}(ad), e:MnO$_2$/Ru^{III}(ad).

in Fig. 30. The MnO$_2$/Pd^{II}(ad) electrode exhibits considerably
high activity comparable to that of the MnO$_2$-Pd(2) electrode.
Besides Pd(II), Pt(IV) as well as Ru(III) also in this type of
electrode contribute to the decrease in chlorine overvoltages.
On the MnO$_2$/Rh^{III}(ad) electrode, the effect of Rh(III) is
hardly detected, quite the same as in the case of the MnO$_2$-Rh(2)
electrode. These noble metal chlorides are considered to
exist as chlorocomplexes in the dilute solutions of hydrochloric
acid [70]. When β-MnO$_2$ is soaked in the chloride solution,
the chlorocomplex of noble metal cation is presumed to be ad-
sorbed on the surface of β-MnO$_2$ accompanied by the surface ion
exchange (or the surface chelation) analogously to the case of
adsorption of ZnCl$_4^{--}$ on the MnO$_2$ powder [71]. For example,
it can be speculated that the Pd(II) ion is attached on the

surface of the β-MnO$_2$ in the following manner:

$$
\begin{array}{c} | \\ Mn-OH \\ O \\ Mn-OH \\ O \\ Mn-OH \\ | \end{array}
\; + \;
\left[\begin{array}{c} Cl \diagdown \diagup Cl \\ \quad Pd^{II} \\ Cl \diagup \diagdown Cl \end{array} \right]^{--}
\; \rightleftarrows \;
\begin{array}{c} | \\ Mn-OH \\ O \\ Mn-O \diagdown \qquad \diagup Cl^{-} \\ \qquad \quad Pd^{II} \\ Mn-O \diagup \qquad \diagdown Cl^{-} \\ | \end{array}
\; + \; 2H^{+} \; + \; 2Cl^{-} \qquad (16)
$$

The potential-time curves on the metal-adsorbed electrodes are shown in Fig. 31.   On the MnO$_2$/Pt^{IV}(ad) electrode the potential shifted to more anodic than 1.4V within several tens of minutes after the start of polarization, while much longer duration was consumed to increase overvoltages on the MnO$_2$/Pd$^{II}_{(ad)}$ and MnO$_2$/Ru^{III}(ad) electrodes.   These anodic shifts in the potentials are due to the desorption of noble metals and the difference in the time required to shift up may be associated with the tightness of the adsorption of each metal.   Therefore, the lower overvoltages in initial periods are caused by the
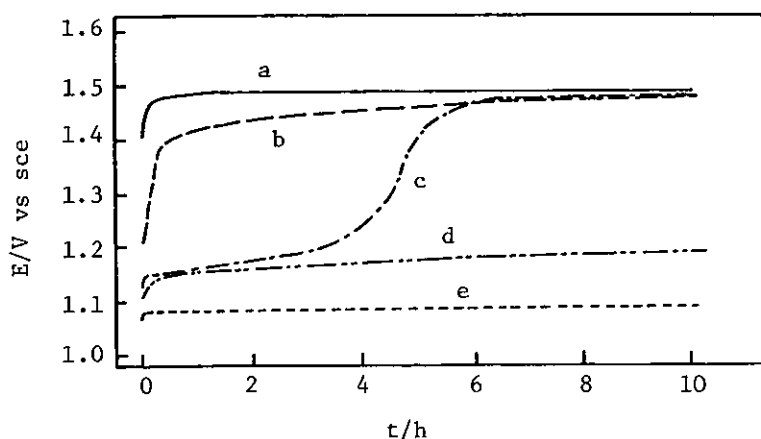

Fig. 31.   Potential-time curves of metal-adsorbed
electrodes at 5mA/cm^2 in 3M NaCl.
a:pure β-MnO$_2$, b:MnO$_2$/Pt^{IV}(ad), c:MnO$_2$/Pd^{II}(ad),
d:MnO$_2$/Ru^{III}(ad), e:metal-doped electrode(MnO$_2$-Pd(2)).

high activities of adsorbed metals for the chlorine evolution reaction.

From the fact that the metal-adsorbed electrodes behave like the metal-doped electrodes, it is considered that even in the case of the metal-doped electrodes noble metal sites exposed at the surface only serve effectively, rather than that the doping effects are resulted from the variation in bulk properties (electronic and/or structural) of β-MnO_2 by doping of noble metals.

The role of doped metals was considered on the basis of Tafel slope (b) and exchange current density (i_0). The Tafel slopes for the anodic evolution of chlorine on the metal-doped electrodes were determined in the low overvoltage region where the concentration polarization could be neglected. The values obtained are summarized in Table 10, in which the data for the corresponding metals (Pd and Pt) and the metal oxides (PdO, PtO_2, RuO_2 and IrO_2) are included. For the chlorine evolution reaction at low overvoltage, two well-known mechanisms have been accepted in general, ie,

Table 10. Tafel slope for the anodic evolution of chlorine

Metal-doped electrode	b(V/dec)	Metal	b(V/dec)	Metal oxide	b(V/dec)
MnO_2-Pd(2)	0.033	Pd	0.033	PdO	0.030
MnO_2-Pt(2)	0.045	Pt	0.042*	PtO_2	0.03[RT/2F]**
MnO_2-Ru(2)	0.055			RuO_2	0.04[2RT/3F]**
MnO_2-Ir(2)	0.057			IrO_2	0.04[2RT/3F]**

* Reference[72]
** Reference[18,20]

$$Cl^- \rightleftharpoons Cl\cdot + e$$

$$2Cl\cdot \rightarrow Cl_2 \qquad (r.d.s.)$$

(17)

and

$$Cl^- \rightleftharpoons Cl\cdot + e$$

$$Cl\cdot + Cl^- \rightarrow Cl_2 + e \qquad (r.d.s.) \ .$$

(18)
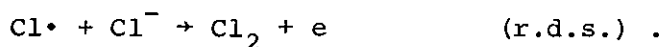
For the mechanisms (17) and (18), one can obtain the theoretical Tafel slopes of 0.03V (RT/2F) and 0.04V (2RT/3F), respectively. It is evident that the chlorine evolution reaction on the MnO_2-Pd(2) electrode proceeds by the mechanism (17), just as on the metal Pd and PdO electrodes. The reaction on the MnO_2-Pt(2) electrode proceeds through the mechanism (18) like on the metal Pt electrode. On the other hand, the values of Tafel slope observed on the MnO_2-Ru(2) and MnO_2-Ir(2) electrodes are larger than that on the MnO_2-Pd(2) electrode. This tendency seems to be in agreement with that in the pure oxide electrodes ($RuO_2 \simeq IrO_2 >$ PdO in Tafel slopes), though each value on the metal-doped electrode does not exactly correspond to that on the pure oxide electrode. Roughly speaking, the mechanism of the chlorine evolution reaction on the noble metal-doped electrode reflects each mechanism on the doped metal or metal oxide electrode.

The exchange current densities, i_0, for the chlorine electrode reaction on metal-doped electrodes are given in Table 3, compared with that on the smooth Pt electrode. The

Table 11. Exchange current density for the
chlorine electrode reaction

Electrode	i_0 (A/cm^2)
MnO_2-Pt(2)	6.8×10^{-2}
MnO_2-Pd(2)	6.1×10^{-2}
MnO_2-Ru(2)	4.1×10^{-2}
MnO_2-Ir(2)	3.8×10^{-2}
smooth Pt	6.7×10^{-3}

i_0 values were calculated from the charge-transfer resistance,
θ, by using the following equation

$$i_0 = \frac{RT}{2F\theta} .$$ (19)

The θ values were determined by Sluyters' method [73] from the
ac impedance measured at the reversible potential (3M NaCl, P_{Cl_2}
= 1atm). The i_0 values shown in Table 11 are reasonable in
magnitudes if the roughness of the electrode surface is taken
into account. Since these oxides were prepared and pretreated
entirely in the same conditions, their true surface areas can
be considered to be approximately the same as each other,
except for the case of the smooth Pt electrode. The i_0 on the
MnO_2-Pt(2) and the MnO_2-Pd(2) electrodes are somewhat larger
than those on the MnO_2-Ru(2) and the MnO_2-Ir(2) electrodes.
This result seems to be compatible with the tendency of the pure
oxides of noble metals where the order of i_0 has been reported
as $PtO_2 \gtrsim PdO > RuO_2 \simeq IrO_2$ [18,69].

From the above discussions on the reaction mechanisms and
the order of the exchange current densities, it is presumed
that the chlorine evolution reaction on the noble metal-doped

- 55 -

electrodes proceed on the sites of doped metals or their oxides. However, other dopants such as Ti, V and Rh did not contribute to activation of β-MnO$_2$ for the chlorine evolution reaction. Probably this is because: (1) the dopant is not effectively dispersed on the electrode surface; or (2) the activity of the doped metal itself is comparable to or lower than that of the β-MnO$_2$. The second reason is more probable.

The current-potential curve on the MnO$_2$-Pd(2) electrode is compared with that on the PdO electrode in Fig. 32. The PdO electrode used was prepared by thermally decomposing PdCl$_2$ at 650°C in O$_2$ atmosphere for 3h, followed by binding PdO powder with Teflon resin (15wt.%). If the doped Pd exist in MnO$_2$ as physical mixture, one can expect that the current density observed at the MnO$_2$-Pd(2) electrode is equal to 2% of that at the PdO electrode. However, it is clear from Fig. 32 that this is not the case.

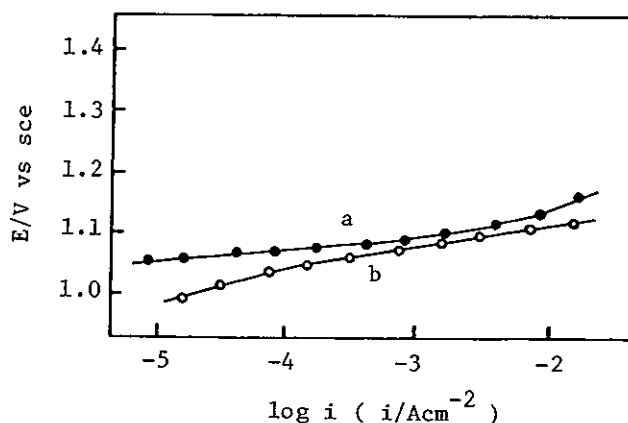There seems to be an activation effect or a synergistic

Fig. 32. Current-potential curves in 3M NaCl.
a:pure PdO, b:MnO$_2$-Pd(2).

effect produced by mixing of the catalysts in the MnO_2-Pd system. This attractive phenomenon might be analogous to that observed on the SnO_2-Pt system [74,75] or on the Pt doped tungsten bronze electrode [76,77]. Accordingly, further details in the mixed Mn-Pd oxide system will be discussed in the next chapter.

4.   SUMMARY

The anodic characteristics of the massive β-MnO_2 doped with noble metals were studied in sodium chloride solution and the results obtained are summarized as follows.

1. The doping of noble metal, especially Pd, decreases the chlorine overvoltage enomously, whereas it scarcely affects the oxygen evolution reaction.

2. The similarity of the polarization characteristics of the doped electrodes to those of the metal-adsorbed electrodes suggests the significance of the noble metal sites exposed at the surface.

3. The data of the Tafel slopes and the exchange current densities also support that the noble metal sites serve as an active site for the chlorine evolution reaction.

CHAPTER 4

THE ELECTROCATALYTIC ACTIVITIES OF THE MIXED Mn-Pd
OXIDES FOR THE CHLORINE EVOLUTION REACTION

1.   INTRODUCTION

Electrocatalysis of metal oxides doped with small amounts
of foreign metals has become of interest in recent years.
There have been many studies, for example, the cathodic reduction
of oxygen on the Pt-doped Na_xWO_3 [76,77] and the anodic evolution
of oxygen and chlorine on the Ru-doped SnO_2 [75,78] or Co_3O_4 [79].
Besides these, it was found in chapter 3 that MnO_2 doped with
the noble metals, especially Pd, exhibits a very high activity
for the anodic evolution of chlorine.   It was also reported
that the addition of MnO_2 in the noble metal oxides or their
mixed oxides decreased the oxygen overvoltage [80] and improved
the anodic durability in chlorate/chloride solution [81].
      Though the active sites for the electrochemical reactions
on these doped (or mixed) electrodes were supposed to be the
noble metal sites, the mechanism of the activation by doping
(or mixing) has been still ambiguous.   Therefore, in this
chapter, the electrocatalytic activity of the Pd-doped massive
MnO_2 was examined for the chlorine evolution reaction in order
to characterize the base metal oxides doped with noble metals
more definitly.   Furthermore, the anodic polarization charac-
teristics of the film-type electrodes of mixed Mn-Pd oxides

were investigated in a sodium chloride solution, in a view of application to the practical electrolysis.

2.   EXPERIMENTAL

The massive MnO_2 electrodes doped with Pd were prepared by the same procedure as that described in chapter 3, and will be referred to as MnO_2-Pd(C_{Pd}), where C_{Pd} represents the concentration of doped Pd in at.% Pd/Mn $(0.2 \leqq C_{Pd} \leqq 5)$.   The X-ray diffraction patterns of the massive electrodes exhibited only that of β-MnO_2 phase and no pattern assigned to Pd or PdO was observed in any case.   A pure PdO electrode made of Teflon-bonded PdO powder was also used as a test electrode for comparison.   These test electrodes were polished with emery papers to present the same condition of the working surface.

The film-type electrodes were prepared by the thermal decomposition method as shown in chapter 1.   A titanium plate (10 x 10 x 0.5mm) was used as a substrate.   Required amounts of aqueous solutions of $Mn(NO_3)_2$, $PdCl_2$ and $RuCl_3$ were mixed together and then applied to one side of the substrate.   The thermal decomposition was carried out at 450°C in air.   The amounts of oxide loadings in the film-type electrodes will be indicated by the value in parentheses in mol of metal/cm^2 for each electrode.

Most of electrochemical measurements were performed by the same procedures as those described in the previous chapters. The anodic current-potential curves for the chlorine evolution

were measured in 3M NaCl or 1M HClO$_4$ + 3M NaCl under the galvanostatic condition. Stirring of the electrolytic solution and elimination of dissolved gases were accomplished by a continuous bubbling of N$_2$. The cathodic current-potential curves for the chlorine reduction were obtained potentiostatically in 1M HClO$_4$ saturated with 1atm Cl$_2$. These polarization measurements were performed at 30°C. The current densities calculated from the charge transfer resistances in the Faraday impedance [21,73] were used as those for Arrhenius plots to obtain the apparent activation energies. All of current densities shown in this work will be indicated by the apparent one based on the geometric area (1cm^2).

3. RESULTS AND DISCUSSION

1. Electrocatalytic activity of the massive MnO$_2$-Pd electrode

Figure 33 shows the anodic current-potential curves of the MnO$_2$-Pd electrodes in 3M NaCl + 1M HClO$_4$. An anodic Tafel slope, b$_a$, of 0.03V was observed on the highly doped electrodes (C$_{Pd}$ = 2 and 5). On the other hand, the curves obtained on the lower Pd-content electrodes had not well-defined Tafel regions. The steep bending of the curves shown in the more anodic region seems to be attributable to change in the surface coverage by the reaction intermediate rather than to contribution of the concentration polarization as reported for the Pt electrode [82]. This will be further discussed in the
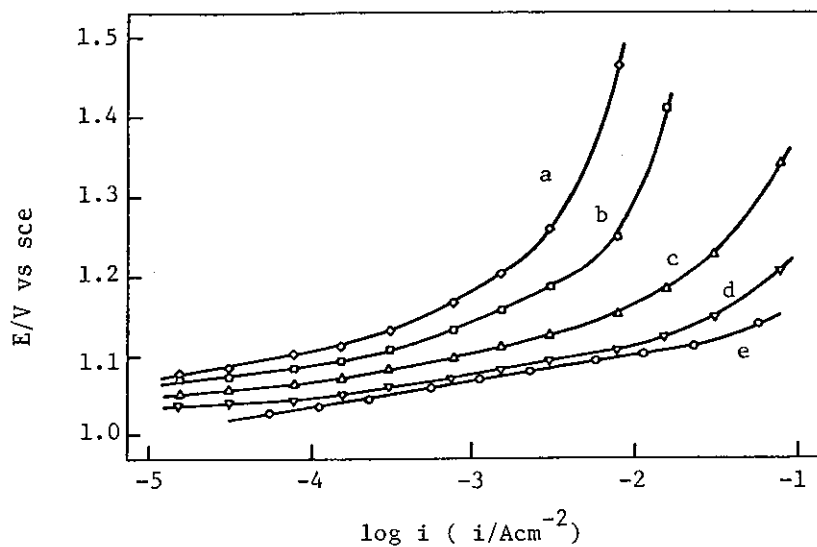
Fig. 33. Current-potential curves of $MnO_2-Pd(C_{Pd})$ electrodes
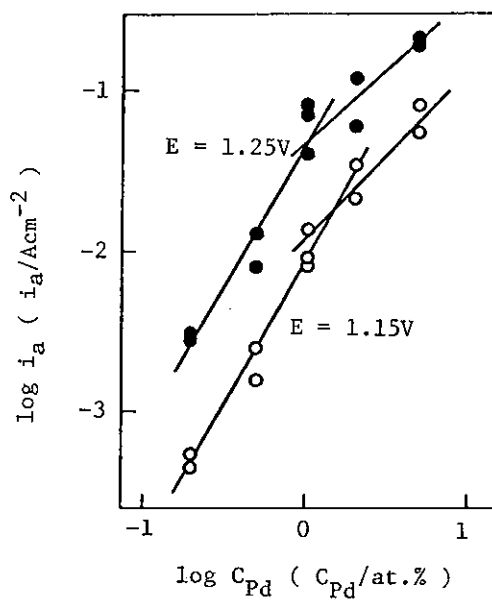in 3M NaCl + 1M $HClO_4$.

C_{Pd} = 0.2(a), 0.5(b), 1(c), 2(d) and 5(e).

Fig. 34. log i_a vs log C_{Pd} plots obtained
from current-potential curves.

later part of this section.

Based on the data of Fig. 33, the current densities, i_a, at E = 1.15V and E = 1.25V are plotted in Fig. 34 against the concentration of doped Pd, C_{Pd}. More than two samples were examined for each C_{Pd} to confirm the reproducibility. Some variance is detectable in the figure, suggesting that the C_{Pd} in the oxide bulk does not closely reflect the concentration of Pd at the electrode surface, but, as a whole, log i_a increases with increasing log C_{Pd}. The current density, or the catalytic activity, tends to saturate in the high C_{Pd} region. The slopes of the lines shown in Fig. 34 are 1.8 and 1.0 at low C_{Pd} and high C_{Pd}, respectively.

Figure 35 shows the cathodic current-potential curves in 1M $HClO_4$. The oxide itself (MnO_2 and/or PdOx) is scarcely reduced in this potential region as shown by curve (f) in the figure. The cathodic limiting currents in curves (a) - (e)
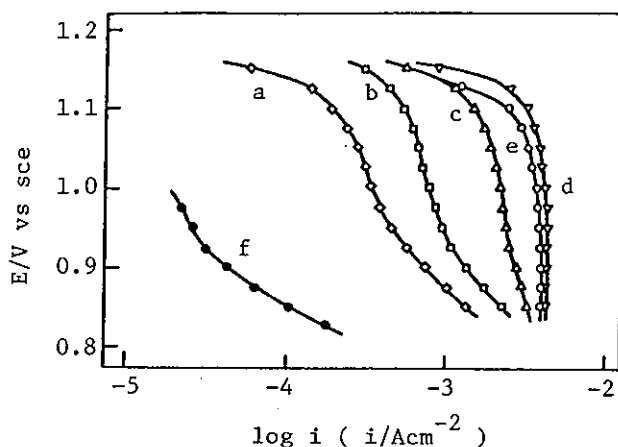

Fig. 35. Current-potential curves of MnO_2-Pd(C_{Pd}) electrodes in Cl_2-saturated 1M $HClO_4$ (a-e) and in N_2-saturated 1M $HClO_4$ (f). C_{Pd} = 0.2(a), 0.5(b), 1(c), 2(d) and 5(e,f).

suggest that the chlorine reduction reaction on these electrodes is controlled by the step of the dissociative adsorption of chlorine. It is considered that the bending of the curves at more cathodic potential, especially on the low C_{Pd}-electrodes, is due to somewhat contribution of the reduction current of the oxide itself or to overapping of the chlorine reduction on the MnO_2.

The plots of $\log i_c$ vs $\log C_{Pd}$ are shown in Fig. 36 based on the data of Fig. 35. In the high C_{Pd} region, $\log i_c$ tends to saturate with increasing $\log C_{Pd}$ while the relation between i_c and C_{Pd} in the low C_{Pd} region is approximately of first-order. It is apparent from this figure that the dissociative adsorption of chlorine takes place at the Pd site preferentially. If the cathodic limiting current reflects the number of the Pd sites at the electrode surface, Fig. 36 indicates the relation
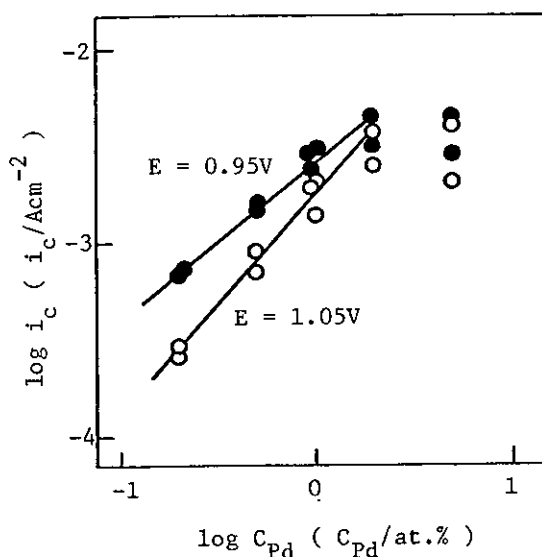

Fig. 36. $\log i_c$ *vs* $\log C_{Pd}$ plots obtained from current-potential curves.

between the bulk concentration of the doped Pd (C_{Pd}) and the number of the effective sites for the chlorine electrode reaction within the exposed Pd sites at the electrode surface (i_c). Figure 37 shows the plot of log i_a (at E = 1.15V in Fig. 34) vs log i_c (at E = 1.05V in Fig. 36) for all electrodes examined. A good linear relation with a slope of 2.0 is detectable not only in the low C_{Pd} (ie low i_c) region but also in the high C_{Pd} (ie high i_c) region, in contrast to the relations shown in Figs. 34 and 36. The linearity of the data in Fig. 37 suggests that the saturation of the current densities in the high C_{Pd} region observed in Figs. 34 and 36 is caused by the non-linear relation between the number of the effective Pd sites at the
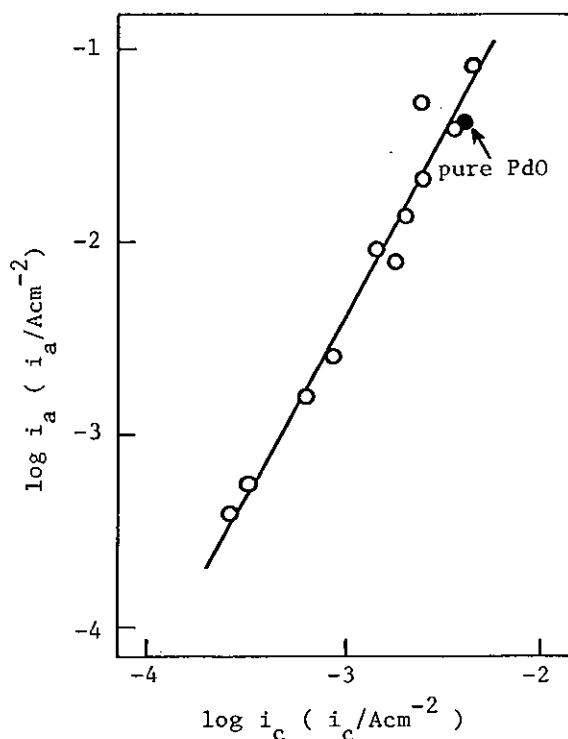

Fig. 37. log i_a *vs* log i_c plot obtained from Figs. 34 and 36.

surface and the Pd concentration in the oxide bulk. The absolute number of the Pd sites exposed at the surface was not measured directly. But it must be proportional to the bulk concentration of the doped Pd, because any result suggesting heterogeneity of the doped Pd in the oxide was not obtained. That is, it was confirmed that any significant dispersion of the data was not observed in the different electrode surfaces prepared by cutting off the massive samples with the emery papers. The saturation of the current densities observed in Figs. 34 and 36 eventually means that the fraction of the effective sites for participating in the chlorine electrode reaction decreases with increasing C_{Pd} within all the exposed Pd sites at the electrode surfaces.

From the results, $b_a = 0.03V$ and $b_c = -\infty$ at the relatively low overvoltages, as shown in Figs. 33 and 35, the chlorine electrode reaction on the MnO_2-Pd electrodes seems to proceed with so-called catalytic mechanism (Volmer-Tafel mechanism), equation (20) and (21),

$$Cl^- \rightleftharpoons Cl\cdot\ +\ e \qquad\qquad (20)$$

$$2Cl\cdot\ \leftrightarrow\ Cl_2 \qquad\qquad (21)$$

where equation (21) is the rate determining step. For the anodic reaction, the current density can be expressed by equation (22),

$$i_a = k_a [Cl\cdot]^2 \qquad\qquad (22)$$

where [Cl·] is the concentration of the reaction intermediate,

Cl·, per unit surface area, and is a function of the electrode potential, E, the concentration of Cl^- ion in the electrolyte, C_{Cl^-}, the number of the available active sites, N_{Pd}, and the degree of their coverage with Cl·, $\theta_{Cl·}$. If C_{Pd} is altered under a condition of constant E and C_{Cl^-}, [Cl·] is given by

$$[Cl·] = \theta_{Cl·} N_{Pd} \quad , \tag{23}$$

and then equation (22) can be rewritten in equation (24),

$$i_a = k_a \theta_{Cl·}^2 N_{Pd}^2 \quad . \tag{24}$$

For the cathodic reaction,

$$i_c = k_c N_{Pd}/2 \quad . \tag{25}$$

From equations (24) and (25), it can be deduced that

$$i_a = k \theta_{Cl·}^2 i_c^2 \quad , \tag{26}$$

where $k = 4k_a/k_c^2$. By comparing equation (26) with the experimental result of $i_a \propto i_c^2$ shown in Fig. 37, it is proved that $\theta_{Cl·}$ is kept constant during the variation of C_{Pd}. Consequently, $\theta_{Cl·}$ is not defined for all Pd sites exposed at the surface but for the effective Pd sites for participating in the chlorine electrode reaction.

The proportionality between C_{Pd} and N_{Pd} in the low C_{Pd} region as shown in Fig. 36 indicates that the increase in the Pd content causes to increase the number of the active particles holding the particle diameter constant in the oxide [77]. This means that the active particles involving Pd are dispersed with microscopic homogeneity. If the area of the active

portion containing the Pd particles increases simply with C_{Pd}
(or, if the doped Pd has a macroscopic structure as metal Pd
or PdO), the relation of $i_a \propto C_{Pd}$ as well as $i_c \propto C_{Pd}$ should
be observed experimentally.   This is not the case.   The
results show that the increase in C_{Pd} leads to the increase in
the number of the active sites per unit area on the atomic
scale.   The saturation of N_{Pd} in the high C_{Pd} region (in
Fig. 35) seems to be attributable to that the dimensions of
the active particles containing Pd grow with increase in C_{Pd}
and that the particles become to have macroscopic structures
as metal Pd or PdO.   The relation between i_a and i_c on the
tablet-type pure PdO electrode, which is also indicated in
Fig. 37, is satisfied with the relation obtained on the MnO_2-
Pd system.   From the comparison of the reaction rate on the
pure PdO electrode with that on the MnO_2-Pd electrode, it is
assumed that the fraction of the uneffective sites for partici-
pating in the chlorine electrode reaction (the dead sites)
is increased within all Pd sites at the surface even on the
high C_{Pd}-electrodes as well as on the pure PdO electrode.
The role of the MnO_2 as a support of the active catalyst, which
is more significant in the low C_{Pd} region, is to disperse the
Pd particles effectively on the atomic scale.

A typical dependence of the chlorine evolution reaction
on the concentration of Cl^- ions is shown for the MnO_2-Pd(1)
electrode in Fig. 38.   Substantially analogous results were
obtained on the other electrodes.   By assuming the Langmuir
adsorption isotherm one obtains
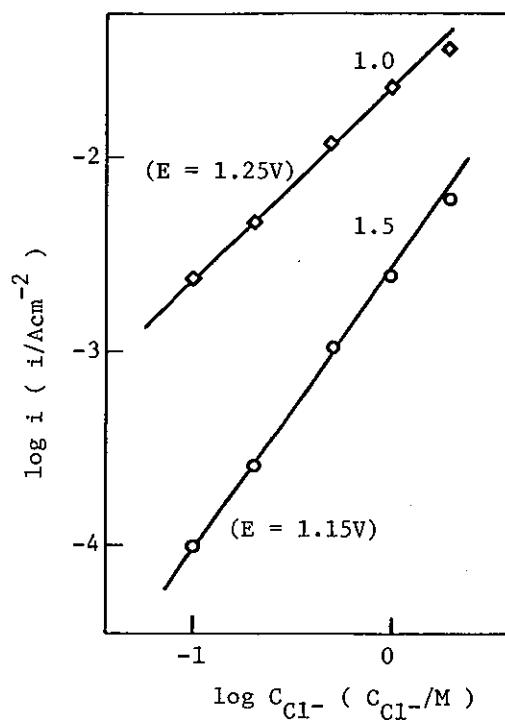
Fig. 38. Dependence of anodic current density
on Cl^- ion concentration.

$$\theta_{Cl\cdot} = \frac{KC_{Cl^-}\exp(EF/RT)}{1 + KC_{Cl^-}\exp(EF/RT)} \qquad (27)$$

where K is the quasi-equilibrium constant for equation (20).
From equations (24) and (27),

$$i_a \propto \left[\frac{KC_{Cl^-}\exp(EF/RT)}{1 + KC_{Cl^-}\exp(EF/RT)}\right]^2 , \qquad (28)$$

and then equation (28) can be replaced by equation (29) for
convenience,

$$i_a \propto C_{Cl^-}{}^n \qquad (29)$$

In this equation n is exactly equal to 2 for $\theta_{Cl\cdot} \to 0$ but it changes continuously from 2 to 0 with increasing $\theta_{Cl\cdot}$ (or E). The result shown in Fig. 38 means that the $\theta_{Cl\cdot}$'s have relatively large values at the measured potentials. The reaction order of 1.0 with respect to Cl^- ion at 1.25V can be also derived from the processes in which the primary Cl^- ion discharge step, equation (20), is rate-determining, but the retention of the relation of $i_a \propto [Cl\cdot]^2$ even at this potential (Fig. 34) strongly suggests that the recombination step, equation (21), is still rate-controlling.

Figure 39 shows the Arrhenius plots of the current densities for the chlorine evolution reaction. The apparent activation energies were calculated from the slopes of the straight lines in the figure and are summarized in Table 12. It is
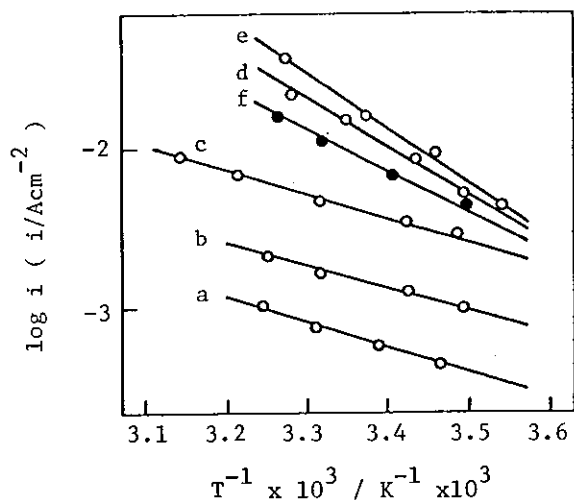

Fig. 39. Arrhenius plots for Cl_2 evolution on MnO_2-Pd(C_{Pd}) electrodes and pure PdO electrode.
C_{Pd} = 0.2(a), 0.5(b), 1(c), 2(d) and 5(e). pure PdO(f).

Table 12.

Apparent activation energy for the

chlorine evolution reaction (E = 1.15V)

Electrode	Activation energy ($kj \cdot mol^{-1}$)
MnO_2-Pd(0.2)	31.9
(0.5)	26.8
(1)	29.3
(2)	57.3
(5)	66.9
Pure PdO	49.7

qualitatively proved that there is a difference in the activation
energies between the low C_{Pd}-electrodes (C_{Pd} = 0.2, 0.5 and 1)
and the high C_{Pd}-electrodes (C_{Pd} = 2 and 5). This distinction
in the activation energies seems to correspond to the definite
break in the log i_a vs log C_{Pd} plots shown in Fig. 34. An
activation energy is one of the kinetic parameters in which any
factor with respect to the real surface area of the electrode
(or the number of active sites at the electrode) is not included,
and it reflects the details of the reaction mechanism [83].
The relatively high values of the activation energies observed
on the high C_{Pd}-electrodes are approximately equal to that on
the pure PdO electrode, and then it suggests that on these
electrodes not only the macroscopic reaction mechanisms but
also the energy states of the reaction intermediates are similar
to each other. On the other hand, the activation energies
observed on the low C_{Pd} electrodes are relatively low. This
result leads to the supposition that the energetic surroundings
of the reaction intermediates on the low C_{Pd}-electrodes are
appreciably different from that on the pure PdO electrode.

Because of the complexity of the electrode system, it is difficult to explain quantitatively the activation energy obtained on this type of electrode. However, the following qualitative concept may be present. On the MnO_2-Pd electrodes possessing low C_{Pd}, there are many Mn sites around the active Pd sites which are homogeneously dispersed on the atomic scale. The reaction rate of the primary Cl^- ion discharge step, equation (20), on the Mn site is considerably slower than on the Pd site. Thus the surface concentrations of Cl· on the low C_{Pd}-electrodes are held extremely low on the whole electrode surface, and are different from those on the high C_{Pd} or pure PdO electrode. The low values of the activation energy can be correlated with the instability in the state of the intermediate Cl·. As the Cl· on the Mn site is considered to be unstable, the process may involve a certain specific step such a spillover step [77] of the Cl· from the Pd site to the Mn site. Somewhat similar mechanism with the heterogeneous recombination of the intermediates on the different kind of sites has been already reported by Furuya and Motoo [84] for the hydrogen evolution reaction on the metal electrodes attaching adatoms.

2. Anodic characteristics of the film-type electrodes of mixed Mn-Pd oxides

Figure 40 shows the anodic polarization curves of the Ti/PdOx(10^{-6}), Ti/MnOx(8×10^{-6})-PdOx(2×10^{-6}) and Ti/MnOx(8×10^{-6})-RuOx(2×10^{-6}) electrodes. The curve for the Ti/MnOx-PdOx electrode is fairly different from that for the Ti/MnOx-RuOx
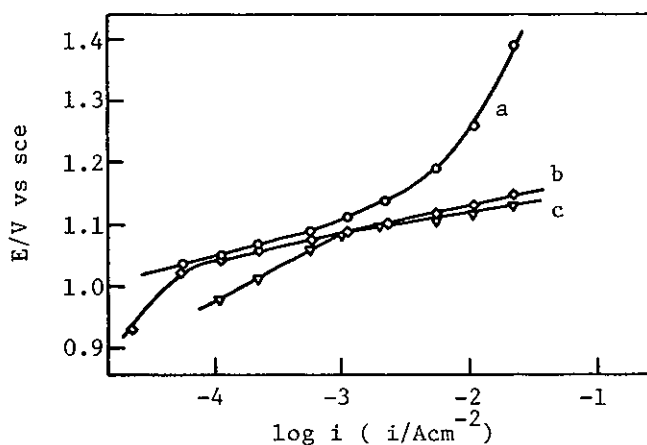
Fig. 40. Current-potential curves of Ti-supported
          electrodes.
          a:Ti/MnOx(8×10^{-6})-PdOx(2×10^{-6})
          b:Ti/MnOx(8×10^{-6})-RuOx(2×10^{-6})
          c:Ti/PdOx(10^{-6})

electrode and the catalytic activity of the former electrode
is much inferior to that of the Ti/PdOx electrode.   For these
reasons, the followings can be pointed out.   In the case of
the Ti/PdOx electrode, the active layer consists of PdO and a
small amount of metallic Pd [85], which contributes to both
the adhesion of the active layer to the Ti substrate and the
electric conductivity in the region of the Ti/PdOx interface.
On the other hand, in the case of the Ti/MnOx-PdOx electrode,
the addition of MnOx in PdOx causes the growth of the insulating
TiO_2 on the Ti substrate in the same manner as in the Ti/MnOx
electrodes, and the metallic Pd coexisting in the active layer
is also oxidized to PdO completely because of the strong
oxidizing atmosphere induced by the presence of MnOx.   These
lead to the decrease in the electric conductivity, and hence
the addition of MnOx to PdOx is rather undesirable for the

anodic characteristics of the Ti-supported electrodes.   In

contrast to the mixed oxides of Mn and Pd, RuOx mainly composed

of RuO_2 has a high conductivity [86-88] as well as its high

solubility in TiO_2 [3,16,42,44,89] enough to provide the high

electric conductivity of the Ti/MnOx-RuOx electrode.   Thus,

the high catalytic activity of RuOx for the chlorine evolution

reaction appears even in the case of the Ti/MnOx-RuOx electrodes.

That is to say, the poor electrical property of the Ti/MnOx

preferencially appears in that of the Ti/MnOx-PdOx electrodes,

while the good electrical and electrochemical properties of the

Ti/RuOx are strongly reflected in those of the Ti/MnOx-RuOx

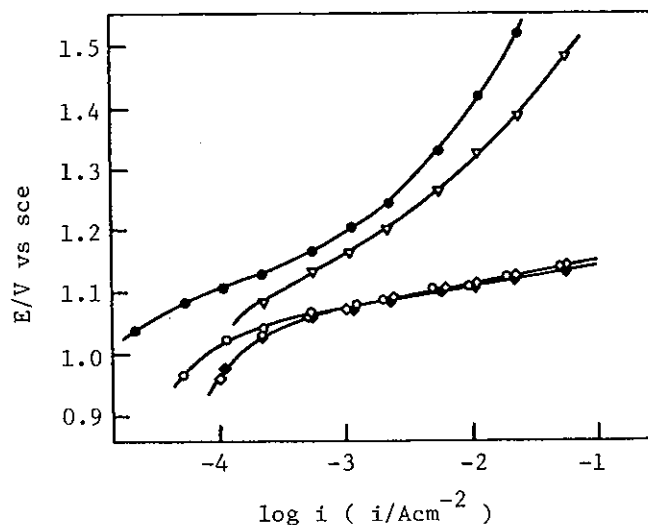electrodes.

Fig. 41.   Current-potential curves of Ti/RuOx-supported
           electrodes.
           ● :Ti/RuOx($2x10^{-8}$)
           ▼ :Ti/RuOx($2x10^{-8}$)/MnOx(10^{-5})
           ○ :Ti/RuOx($2x10^{-8}$)/MnOx(10^{-5})-PdOx(10^{-7})
           ◇ :Ti/RuOx($2x10^{-8}$)/MnOx(10^{-8})-PdOx($2x10^{-7}$)
           ◆ :Ti/RuOx($2x10^{-8}$)/PdOx($2x10^{-7}$)

In order to minimize the catalytic activity of RuOx in the mixed oxide system, the thermal decomposition was carried out in two stages for the electrode preparation. The Ti substrate was at first coated with thin film of RuOx (2×10^{-8} mol/cm^2) and then with layer of MnOx and/or PdOx. The current-potential curves of the resulted electrodes are shown in Fig. 41. The Ti/RuOx(2×10^{-8}) electrode showed somewhat lower activity owing to the insufficient amount of the catalyst loadings. The Ti/RuOx(2×10^{-8})/MnOx(10^{-5}) electrode, whose active layer was predominantly composed of MnOx, was more active than the Ti/RuOx electrodes, but much less active than the PdOx-containing electrode. It is considered that the low chlorine overvoltage of the Ti/RuOx/MnOx-PdOx electrodes is attributable to high electric conductivity of the RuO$_2$ in the region of the Ti substrate/active layer interface. By comparing the polarization curves of the Ti/RuOx/PdOx and Ti/RuOx/MnOx-PdOx electrodes, however, it became apparent that the existence of MnOx in the catalyst hardly affects the catalytic activity in this system.

The results for the Ti/MnOx-RuOx electrodes shown in Fig. 40 suggest that RuOx coexisting in the Ti/MnOx still keeps high conductivity. Therefore, the improved conductivity could be expected for the Ti/MnOx-PdOx-RuOx electrodes if they were prepared by the simultaneous thermal decomposition of mixed solutions of Mn(NO$_3$)$_2$, PdCl$_2$ and RuCl$_3$. The polarization curves of the resulted electrode and the relating electrodes are shown in Fig. 42. The amounts of PdOx loadings are 10^{-7} mol/cm^2, while that of MnOx loading is 10^{-5} mol/cm^2. It is evident from this figure that the PdOx existing in the active
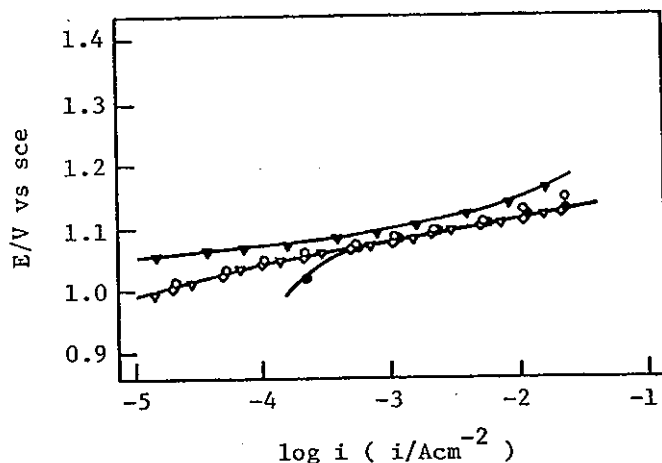
Fig. 42.   Current-potential curves of massive
           and Ti-supported electrodes.
           ▼:tablet-type PdO
           ▽:massive MnO_2-Pd(2)
           o:Ti/MnOx(10^{-5})-PdOx(10^{-7})-RuOx(10^{-7})
           ●:Ti/PdOx(10^{-7})
           ◇:Ti/PdOx(10^{-7})-RuOx(10^{-7})

layer specially serves as an active catalyst for the anodic

evolution of chlorine.   Though it has already been well-known

that RuO_2 is one of the most active catalysts for this reaction

[11-22], any decrease in the overvoltage by addition of RuOx

in PdOx was not observed on the Ti/PdOx-RuOx electrode.   The

data on the massive MnO_2 electrodes, included in Fig. 42, showed

that the activity of the massive MnO_2 doped with 2atom.% Pd,

MnO_2-Pd(2) electrode, was superior to that of the tablet-type

pure PdO electrode.   However, the expected synergistic effects

were not observed in the case of the film-type electrodes.

Such different results are probably due to the difference in

dispersing conditions of Pd (or PdOx) and specific surface areas

of catalysts.   It is also possible to consider that the TiO_2

formed in the Ti/PdOx electrode plays the role which the MnO_2 does in the massive MnO_2-Pd electrode. That is, the Pd site might be dispersed in a relatively small amount of the TiO_2 on the substrate, in analogy with the Pd in the massive MnO_2.

Consequently, any unambiguous evidence of synergistic effects was not observed in the film-type Mn-Pd mixed oxide electrodes because of the complexity of the electrode system. However, it was at least suggested from the results obtained with the massive electrodes that more effective configuration of the active sites becomes feasible by introducing the active catalyst into inactive one. Thus, from these viewpoints, the introduction of other components into various kinds of oxides will be investigated with great interest.

4.   SUMMARY

The electrocatalytic activities of the mixed Mn-Pd oxides were examined for the chlorine evolution reaction. The results obtained in this chapter are summarized as follows.

1. A second order relation observed on the massive MnO_2-Pd between the rate of the chlorine evolution and the number of the surface Pd sites suggested strongly that the active sites are more effectively dispersed on the MnO_2 surface with microscopic homogeneity.

2. From the data of the activation energies, it was also supported that the reaction mechanism on the lower doped MnO_2-Pd is somewhat different from that on the pure PdO electrode.

3. In the case of the film-type Mn-Pd oxides, however, any distinct evidence of synergistic effects was not observed because of the complexity of the electrode system and of the high activity of the PdOx film itself.

CONCLUSION

The author carried out the studies on the anodic character-
istics of manganese oxides in aqueous solutions.   The main
results and conclusions obtained in this work are summarized as
follows.

1.   The film-type manganese oxides, MnOx, supported with
conductive substrates such as Pt and RuOx-coated Ti exhibit a
relatively high activity for the anodic evolution of oxygen.
The process of the primary water or hydroxide ion discharge is
rate-determining in the oxygen evolution reaction on the MnOx
film electrodes.

2.   The redox reaction of Mn(III)/Mn(IV) in the massive
manganese oxides is characterized by accompanying the diffusion
of H^+ ions in the solid phase.   The active site for the oxygen
and chlorine evolution reaction is regarded as the Mn(III) site
at the surface, and the oxidation process of the Mn(III) site
is considered to be a common rate-determining step in both
reactions on the massive manganese oxides.

3.   The doping of small amounts of noble metals, especially
Pd, in the massive β-MnO$_2$ decreases the chlorine overvoltage
enomously.   The kinetic data suggest that the surface sites
of the doped metals serve as an active site for the chlorine
evolution reaction.

4.   In the case of the massive MnO$_2$-Pd electrodes, the
active Pd sites are effectively dispersed on the MnO$_2$ surface
with microscopic homogeneity, and the kinetics of the chlorine

evolution reaction, especially on the lower Pd-doped MnO_2, is somewhat different from that on the pure PdO electrode.   In the case of the film-type Mn-Pd mixed oxides, however, the catalytic activity is not improved by mixing of the oxides.

ACKNOWLEDGMENT

REFERENCES

1. A.T. Kuhn and P.M. Wright, "Industrial Electrochemical Processes" (ed. by A.T. Kuhn), p. 525, Elsevier Pub. Co., New York (1971).

2. eg. H.B. Beer, Belg. Pat. 710,551 (1968); O.de Nora, South African Pat. 68/7371, 68/7482 (1968).

3. O.de Nora, Chem. Ing. Techn., $\underline{42}$, 222 (1970).

4. G. Bianchi, J. Appl. Electrochem., $\underline{1}$, 231 (1971).

5. I.E. Veselovskaya, L.V. Morochko, L.I. Yurkov and L.M. Yakimenko, Élektrokhimiya, $\underline{10}$, 1017 (1974).

6. G. Faita, P. Longhi and T. Mussini, J. Electrochem. Soc., $\underline{114}$, 340 (1967).

7. G. Faita, G. Fiori and J.W. Augustynski, J. Electrochem. Soc., $\underline{116}$, 928 (1969).

8. G. Faita, G. Fiori and A. Nidora, J. Electrochem. Soc., $\underline{117}$, 1333 (1970).

9. R.T. Atanasoski, B.Ž. Nikolić, M.M. Jaksić and A.R. Despić, J. Appl. Electrochem., $\underline{5}$, 155 (1975).

10. T. Arikado, C. Iwakura and H. Tamura, Electrochim. Acta, $\underline{22}$, 229 (1977).

11. G. Faita and G. Fiori, J. Appl. Electrochem., $\underline{2}$, 31 (1972).

12. E.A. Kalinovskii, R.U. Bondar' and N.N. Meshkova, Élektrokhimiya, $\underline{8}$, 1468 (1972).

13. R.G. Erenburg, L.I. Kristalik and V.I. Bystrov, Élektrokhimiya, $\underline{8}$, 1740 (1972).

14. V.I. Bystrov, Élektrokhimiya, $\underline{11}$, 1902 (1975).

15. N.Ya. Buné, G.A. Shilyaeva and V.V. Losev, Élektrokhimiya, 13, 1540 (1977).

16. F. Hine, M. Yasuda and T. Yoshida, J. Electrochem. Soc., 124, 500 (1977).

17. L.J.J. Janssen, L.M.C. Starmans, J.G. Visser and E. Barendrecht, Electrochim. Acta, 22, 1093 (1977).

18. T. Arikado, C. Iwakura and H. Tamura, Electrochim. Acta, 23, 9 (1978).

19. J. Augustynski, L. Balsenc and J. Hinden, J. Electrochem. Soc., 125, 1093 (1978).

20. I.R. Burrows, D.A. Denton and J.A. Harrison, Electrochim. Acta, 23, 493 (1978).

21. D.A. Denton, J.A. Harrison and R.I. Knowles, Electrochim. Acta, 24, 521 (1979).

22. L.D. Burke and J.F. O'Neill, J. Electroanal. Chem., 101, 341 (1979).

23. M. Takahashi and N. Masuko, "Kogyodenkai no Kagaku", Chap. 9, Agune, Tokyo (1979).

24. W. O'Grady, C. Iwakura, J. Huang and E. Yeager, "Proceedings of the Symposium on Electrocatalysts" (ed. by M.W. Breiter), p. 286, The Electrochemical Society, New Jersey (1974); Technical Report, No. 37, Case Western Reserve University, 1 May (1974).

25. C. Iwakura, K. Hirao and H. Tamura, Electrochim. Acta, 22, 335, (1977).

26. C. Iwakura, H. Tada and H. Tamura, Denki Kagaku, 45, 202 (1977).

27. L.D. Burke, O.J. Murphy, J.F. O'Neill and S. Venkatesan,
     J. Chem. Soc. Faraday 1, 73, 1659 (1977).

28. G. Lodi, E. Sivieri, A.de Battisti and S. Trasatti,
     J. Appl. Electrochem., 8, 135 (1978).

29. D.V. Kokoulina, Yu.I. Krasovitskaya and T.V. Ivanova,
     Élektrokhimiya, 14, 470 (1978).

30. M.A. Malati, Chem. Ind. (London), 17, 446 (1971).

31. W.C. Vosburg, J. Electrochem. Soc., 106, 839 (1959);
     A. Kozawa and R.A. Powers, J. Electrochem.Soc., 113, 870
     (1966); C.C. Liang, "Encyclopedia of Electrochemistry of
     the Elements" (ed. by A.J. Bard), Vol. I, Chap. 6, p. 349,
     Marcel Dekker, Inc., New York (1973).

32. G.N. Kokhanov, R.A. Anganova and N.G. Milova, Élektrokhimiya,
     8, 862 (1972).

33. E.M. Shembel', E.A. Kalinovskii, V.L. Moskalevich,
     O.M. Mazur and V.G. Artamonov, Élektrokhimiya, 8, 1351
     (1972).

34. E.A. Kalinovskii, V.A. Shustrov, V.M. Chaikovskaya and
     O.L. Prusskaya, Élektrokhimiya, 12, 1573 (1976).

35. A.K. Gorbachev, É.É. Krench and V.I. Shmorgun,
     Élektrokhimiya, 13, 1046 (1977).

36. R. Mráz, V. Srb and S. Tichý, Electrochim. Acta, 18, 551
     (1973).

37. M.B. Konovalov, E.A.Kalinovskii, A.F. Nikiforov and
     V.V. Stender, Khim. Teknologiya, 17, 101 (1971).

38. C. Iwakura, K. Fukuda and H. Tamura, Electrochim. Acta,
     21, 501 (1976).

39. A.K. Covington, T. Cressey, B.G. Lever and H.R. Thirsk, Trans. Faraday Soc., 58, 1975 (1962).

40. A. Kozawa and W.C. Vosburgh, J. Electrochem. Soc., 105, 59 (1958).

41. C. Butler and H.R. Thirsk, J. Electrochem. Soc., 100, 297, (1953).

42. I.E. Veselovskaya, E.K. Spasskaya, V.A. Sokolov, V.I. Tkachenko and L.M. Yakimenko, Élektrokhimiya, 10, 70, (1974).

43. H. Tamura, H. Yoneyama, C. Iwakura and T. Murai, Bull. Chem. Soc. Jpn., 50, 753 (1977).

44. K. Fukuda, C. Iwakura and H. Tamura, Abstract(1K45) presented at 36th Spring Meeting of the Chemical Society of Japan, April (1977).

45. M. Valigi and A. Cimino, J. Solid State Chem., 12, 135 (1974).

46. "The Oxide Handbook" (ed. by G.V. Samsonov), p. 25,28, Plenum Pub. Co., New York (1973).

47. "Kagaku Binran" (ed. by Chemical Society of Japan), p. 1423, Maruzen, Tokyo (1975).

48. H.Y. Kang and C.C. Liang, J. Electrochem. Soc., 115, 6 (1968).

49. H.S. Harned and M.A. Cook, J. Am. Chem. Soc., 59, 496 (1937).

50. J.O'M. Bockris, J. Chem. Phys., 24, 817 (1956).

51. A. Damjanovic, A. Dey and J.O'M. Bockris, Electrochim. Acta, 11, 791 (1966).

52. Y. Yoneda, J. Electrochem. Soc. Japan, 22, 266 (1949).

53. A. Hickling and S. Hill, Discuss. Faraday Soc., $\underline{1}$, 236 (1947).

54. R. Naumann, Ch. Hirche and G. Wolf, Z. Phys. Chem., $\underline{257}$, 697 (1976).

55. J.S. Wiley and H.T. Knight, J. Electrochem. Soc., $\underline{111}$, 656 (1964).

56. P.H. Klose, J. Electrochem. Soc., $\underline{117}$, 854 (1970).

57. T. Arikado, C. Iwakura and H. Tamura, Electrochim. Acta, $\underline{22}$, 513 (1977).

58. R.S. Nicholson and I. Shain, Analyt. Chem., $\underline{36}$, 706 (1964).

59. H.R. Thirsk and J.A. Harrison, "A Guide to the Study of Electrode Kinetics", Chap. 2, p. 52, Academic Press, London (1972).

60. T. Valand, Electrochim. Acta, $\underline{19}$, 639 (1974).

61. J.J. Larange and J. Brenet, Bull. Soc. Chim. Fr., $\underline{7}$, 2455 (1970).

62. A.B. Scott, J. Electrochem. Soc., $\underline{107}$, 941 (1960).

63. G. Faita, G. Fiori and T. Mussini, Electrochim. Acta, $\underline{13}$, 1765 (1968).

64. T. Yokoyama and M. Enyo, Abstract(A124) presented at the 43rd Annual Meeting of the Electrochemical Society of Japan, April (1976).

65. S.M. Ahmed and D. Maksimov, Can. J. Chem., $\underline{46}$, 3841 (1968).

66. A. Kozawa, Abstract(D116) presented at the 44th Annual Meeting of the Electrochemical Society of Japan, April (1977).

67. S. Gottesfeld and S. Srinivasan, J. Electroanal. Chem., $\underline{86}$, 89 (1978).

68. G. Singh, M.H. Miles and S. Srinivasan, "Electrocatalysis on Non-Metallic Surfaces" (ed. by A.D. Franklin), p. 289, National Bureau of Standards, Maryland (1976).

69. M. Takahashi, Hyomen, $\underline{12}$, 170 (1974).

70. F.A. Cotton and G. Wilkinson, "Advanced Inorganic Chemistry" Chap. 30, Wiley, New York (1966).

71. A. Kozawa, J. Electrochem. Soc., $\underline{106}$, 552 (1959).

72. I.R. Burrows, J.H. Entwisle and J.A. Harrison, J. Electroanal. Chem., $\underline{77}$, 21 (1977).

73. J.H. Sluyters, Rec. Trav. Chim., $\underline{79}$, 1092 (1960).

74. M.R. Andrew, J.S. Drury, B.D. McNicol, C. Pinnington and R.T. Short, J. Appl. Electrochem., $\underline{6}$, 99 (1976).

75. C. Iwakura, M. Inai and H. Tamura, Chem. Lett., $\underline{1979}$, 225 (1979).

76. J.H. Fishman, J.F. Henry and S. Tessor, Electrochim. Acta, $\underline{14}$, 1314 (1969).

77. J.O'M. Bockris and J. McHardy, J. Electrochem. Soc., $\underline{120}$, 61 (1973).

78. T.A. Chertykovtseva, Z.D. Skuridina, D.M. Shub and V.I. Veselovskii, Élektrokhimiya, $\underline{14}$, 1412 (1978).

79. Ya.M. Kolotyrkin, Extended abstract (No. 19) presented at the 3rd Japan-USSR Seminar on Electrochemistry, Kyoto, December, 1978; Denki Kagaku, $\underline{47}$, 390 (1979).

80. D. Cipris and D. Pouli, J. Electroanal. Chem., $\underline{73}$, 125 (1976).

81. L.M. Elina, V.M. Gitneva and V.I. Bystrov, Élektrokhimiya, $\underline{11}$, 1279 (1975).

82. B.E. Conway and D.M. Novak, J. Electroanal. Chem., 99, 133 (1979).

83. T. Arikado, C. Iwakura and H. Tamura, Electrochim. Acta, 23, 799 (1978).

84. N. Furuya and S. Motoo, J. Electroanal. Chem., 88, 151 (1978).

85. K. Ooe, Y. Kawai and S. Saito, Abstract(B311) presented at the 42nd Annual Meeting of the Electrochemical Society of Japan, April (1975).

86. D.B. Rogers, R.D. Shannon, A.W. Sleight and J.L. Gillson, Inorg. Chem., 8, 841 (1969).

87. S. Pizzini, G. Buzzanca, C. Mari, L. Rossi and S. Torchio, Mat. Res. Bull., 7, 449 (1972).

88. D. Galizziori, F. Tantardini and S. Trasatti, J. Appl. Electrochem., 5, 203 (1975).

89. W.A. Gerrard and B.C.H. Steele, J. Appl. Electrochem., 8, 417 (1978).